# *Melting the hydrous, subarc mantle: the origin of primitive andesites*



**Citation:** Mitchell, Alexandra L., and Timothy L. Grove. "Melting the Hydrous, Subarc Mantle: The Origin of Primitive Andesites." Contributions to Mineralogy and Petrology 170.2 (2015): n. pag.

**As Published:** http://dx.doi.org/10.1007/s00410-015-1161-4

**Publisher:** Springer Berlin Heidelberg

**Persistent URL:** http://hdl.handle.net/1721.1/107271

**Version:** Author's final manuscript: final author's manuscript post peer review, without publisher's formatting or copy editing

# Melting the hydrous, subarc mantle: the origin of primitive andesites

Alexandra L. Mitchell* and Timothy L. Grove

*Department of Earth, Atmospheric and Planetary Sciences,*

*Massachusetts Institute of Technology, Cambridge, MA 02139, USA*

*Email: ala@mit.edu

Keywords: Subduction Zone, Mantle Wedge, Partial Melting, Harzburgite, Experimental Petrology

## *Abstract*

This experimental study is the first comprehensive investigation of the melting behavior of an olivine + orthopyroxene ± spinel - bearing fertile mantle composition as a function of variable pressure and water content. The fertile composition was enriched with a metasomatic slab component of ≤ 0.5% alkalis and investigated from 1,135–1,470˚C at 1.0–2.0 GPa. A depleted lherzolite with 0.4% alkali addition was also studied from 1225-1240˚C at 1.2 GPa. Melts of both compositions were water-undersaturated: fertile lherzolite melts contained 0-6.4 wt% $H_2O$, and depleted lherzolite melts contained ~2.5 wt% $H_2O$. $H_2O$ contents of experimental glasses are measured using electron microprobe (EPMA), secondary ion mass spectrometry (SIMS), and synchrotron-source reflection Fourier transform infrared spectroscopy (ssr-FTIR), a novel technique for analyzing $H_2O$ in petrologic experiments. Using this new dataset in conjunction with results from previous hydrous experimental studies, a thermobarometer and a hygrometer-thermometer are presented to determine the conditions under which primitive lavas were last in equilibration with the mantle. These predictive models are functions of $H_2O$ content and pressure, respectively. A predictive melting model is also presented that calculates melt compositions in equilibrium with an olivine + orthopyroxene ± spinel residual assemblage (harzburgite). This model quantitatively predicts the following influences of $H_2O$ on mantle lherzolite melting: 1) as melting pressure increases, melt compositions become more olivine normative, 2) as melting extent increases, melt compositions become depleted in the normative plagioclase component, and 3) as melt $H_2O$ content increases, melts become more quartz normative.

Natural high–Mg# (molar Mg/ ($Mg+Fe^{2+}$)), high MgO basaltic andesite and andesite lavas—or primitive andesites (PAs)—contain high $SiO_2$ contents at mantle-equilibrated Mg#s.

Their compositional characteristics cannot be readily explained by melting of mantle lherzolite under anhydrous conditions. This study shows that experimental melts of a fertile mantle peridotite plus the addition of alkalis reproduce the compositions of natural PAs in $SiO_2$, $Al_2O_3$, $TiO_2$, $Cr_2O_3$, MgO, and $Na_2O$ at 1.0-1.2 GPa and $H_2O$ contents of 0-7 wt%. Our results also suggest that PAs form under a maximum range of extents of melting from F=0.2-0.3. The CaO contents of the melts produced are 1-5 wt% higher than the natural samples. This is not a result of a depleted source composition or of extremely high extents of melt but is potentially caused by a very low CaO content contribution from deeper in the mantle wedge.

## *Introduction*

Primitive basaltic andesites and andesites with mantle equilibrated Mg#s of $\geq$ 0.7 are found at arcs worldwide (Kelemen et al., 2014). As primitive mantle melts are anticipated to be basaltic in composition (Gaetani and Grove 1998), the anomalously high $SiO_2$ contents (51-59 wt%) of primitive basaltic andesites and andesites have sparked intense debate as researchers have tried to understand how these samples fit into the paradigm of mantle melting at subduction zones. Three models attempt to reconcile the high $SiO_2$ contents of these primitive melts: 1) wet, direct mantle melting (Kushiro et al. 1968; Kushiro 1969, 1972, 1974; Baker et al. 1994; Grove et al. 2002; Grove et al. 2003); 2) assimilation and mixing of primitive basaltic and dacitic melts (Streck et al. 2007; Straub et al. 2008; Straub et al. 2011); and 3) partial melting of subducted material in the eclogite facies followed by assimilation in the mantle wedge (Kay 1978; Tatsumi 2001; Kelemen et al. 2003; Bryant et al. 2010). This study primarily focuses on model 1, followed by a brief assessment of models 2 and 3.

Early on, work on simple systems (CMAS, Fo-Di-$SiO_2$) by Kushiro et al. (1968) and Kushiro (1969, 1970, 1972, and 1974) suggested that water is the key to the generation of high

$SiO_2$ in primitive high-Mg# andesites. Similar studies were subsequently conducted by Nicholls and Ringwood (1972) and Green (1973) and conflicting interpretation of results led to heated debate about the viability of deriving andesites by direct melting of mantle peridotite (Mysen et al. 1974). Kushiro's results, in conjunction with studies investigating the multiple saturation points of natural primitive basaltic andesites and andesites (Tatsumi 1981; Tatsumi 1982; Baker et al. 1994; Grove et al. 2003), suggest that the direct, wet mantle melting model is a viable mechanism for producing basaltic andesites and andesites. Three hydrous experiments by Hirose (1997) successfully produced melt compositions with 54-60 wt% $SiO_2$, though several other hydrous melting studies on more complex systems have not produced the high $SiO_2$ contents of natural primitive lavas (Hirose and Kawamoto 1995; Gaetani and Grove 1998; Falloon and Danyushevsky 2000; Parman and Grove 2004). Instead, these studies have produced basaltic lavas (48-52 wt% $SiO_2$). In this study, we quantify the role of $H_2O$ on the compositions of fertile mantle melts to understand the role of direct, wet mantle melting on the petrogenesis of high Mg# (≥0.70), high MgO (≥ 7 wt%) basaltic andesites and andesites.

## *Experimental Methods*

### *Starting Materials*

#### *Fertile Composition*

The fertile mantle (FM) compositions (Table 1; Mixes A, B, C, D, and E) are mixtures in various proportions of a dry and a wet starting material. The dry composition is an anhydrous powder of Hart and Zindler's 1986 fertile upper mantle (H&Z) plus metasomatic slab components of $Na_2O$ and $K_2O$. The wet composition is the H&Z + $H_2O$ mix of Till et al. (2012b), which contains 14.5 wt% $H_2O$ added as brucite ($Mg(OH)_2$). The FM mixes are made from high purity synthetic oxides; they contain a range of water contents from 0-6 wt% $H_2O$ and

between 0.3 and 0.5% additional alkalis. Alkalis were added to all starting materials because it has been suggested that in the natural system they are added to the mantle wedge from the subducting slab (Stolper and Newman 1994; Pearce and Peate 1995; Grove et al. 2002). Alkalis also significantly (and predictably) affect the compositions of olivine (ol) + orthopyroxene (opx) multiply saturated melts (Kushiro 1975; Grove and Juster 1989).

Dry compositions were conditioned in a 1-atm vertical gas-mixing furnace with $fO_2$ at the QFM buffer for 72 hours at 1050 °C. The wet compositions were not conditioned because doing so would release the $H_2O$ locked up in brucite, which breaks down to periclase + $H_2O$ below 500 °C (Weber and Roy, 1965).

*Depleted Composition*

An anhydrous depleted upper mantle (DM) mix was also synthesized (Table 1). Using the suite of compositionally variable spinel (sp) lherzolites compiled by Herzberg (2004), the MgO content of the DM composition was determined for a depleted CaO content of 2 wt%. The MgO content was then used to find the appropriate values for all other major oxides. The depleted compositions were conditioned in the same method as the dry composition described above—at QFM, 1050 °C for 72 hours in a 1-atm vertical gas-mixing furnace. For depleted mantle experiments, water was added as a liquid via syringe.

*Experimental Methods*

Experiments were performed in a 0.5” end-loaded solid medium piston cylinder (Boyd and England 1960) in the Massachusetts Institute of Technology (MIT) Experimental Petrology Laboratory. Two capsule designs were used: 1) graphite in Platinum and 2) Fe-saturated AuPd. Extended description of experimental methods, experimental conditions, capsule saturation, temperature and pressure calibration, and oxygen fugacity are included in the Experimental Methods Online Supplementary Material.

## *Analytical Techniques*

Data was collected using the Electron Microprobe (EPMA) at MIT (Table 3), secondary ion mass spectrometry (SIMS) at Woods Hole Oceanographic Institute, and synchrotron-source reflection FTIR (ssr-FTIR) at National Synchrotron Light Source (NSLS) at Brookhaven National Laboratories. Detailed discussion of analytical techniques is presented in the Analytical Techniques Online Supplementary Material.

### *Measuring $H_2O$ Contents of Glass*

Because $H_2O$ is difficult to measure in experimental glasses, this study uses three analytical techniques to quantitatively measure the $H_2O$ contents of experimental glasses: EPMA, SIMS, and ssr-FTIR. Using EPMA, $H_2O$ is measured by quantitative analysis of oxygen. Two experiments were measured using SIMS, both had $H_2O$ contents within error of the EPMA measurements. Comparison of the $H_2O$ measurements from all three methods is presented in Table 2 and Figure 2.

Synchrotron-source reflection FTIR has been employed as a novel application to quantitatively measure $H_2O$ in experimentally produced silicate melts. Comparison of $H_2O$ analyses obtained from ssr-FTIR, EPMA, and SIMS indicate that our experiments contain a range of $H_2O$ from ~0.5 to ~7 wt%. The results from EPMA and ssr-FTIR are reproduced within error of one another 60% of the time. The results obtained from ssr-FTIR are also higher than the EPMA results in 69% of experimental glasses analyzed using both methods. Since all glasses contain $H_2O$ measurements from EPMA, and the EPMA results are supported by 60% of the ssr-FTIR results and both of the ion microprobe results, the discussion of this paper uses the EPMA data to examine the effect of $H_2O$ on experimental melts.

### *Measuring $CO_2$ contents of Glasses*

The $CO_2$ content of glasses produced in this study have been measured using ion microprobe and ssr-FTIR. The $CO_2$ content of C470, an experiment conducted in graphite + Pt, was 429 ppm (0.0429 wt%) when measured using the ion microprobe. This measurement is on the same order of magnitude as the $CO_2$ measurement for a run in graphite + Pt by Gaetani and Grove (1998), which contained 0.07 wt% $CO_2$. No $CO_2$ measurements were obtained on the AuPd experiments, though given the results of Gaetani and Grove (1998) on glasses in Fe-saturated AuPd capsules, it is likely that there is ~1.2 wt% $CO_2$ in the AuPd runs. In the ssr-FTIR spectra, however, there were no resolvable peaks at 2350 $cm^{-1}$, the $CO_{2\ mol}$ region, or at 1520 $cm^{-1}$, the $CO_3^{2-}$ doublet, as described by King and Larson (2013) for any of the experiments measured. Given the low $CO_2$ content from the ion microprobe and lack of evidence of $CO_2$ from the ssr-FTIR method, this study assumes that the effect of $CO_2$ in the system is minimal compared to that of $H_2O$.

## *Experimental Results*

### *Phase Equilibria – Fertile Composition*

Seven experiments over the range of pressures investigated (1.0-2.0 GPa) produced a hydrous silicate melt in equilibrium with a harzburgitic residue of ol + opx (Figure 1a). At lower pressures (1.0 and 1.2 GPa), sp was also present in five experiments in addition to ol + opx + melt. Three experiments were saturated in ol + opx + cpx + melt. Two experiments—one with 5.9 wt% $H_2O$ (1.2 GPa, 1215˚C) and one at high temperature (1.2 GPa, 1250˚C, 3.8 wt% $H_2O$) only contained ol + sp + melt. Phase proportions and uncertainties from mass balance calculations using the LIME program (Krawczynski and Olive 2011) are reported in Table 2.

As expected, experiments with ol + sp + melt contained the highest melt fractions at 39% (C553) and 44% (C559) due to the higher $H_2O$ content and the higher temperature of the run,

respectively (Figure 1b). For runs saturated with ol + opx, the melt fraction was close to 30% for all runs except for one at 1.0 GPa, which contained 23% melt. The melt fraction of runs with ol + opx + sp + melt was more variable with melt extents ranging from 27% to 38%, and the three experiments saturated with ol + opx+ cpx all contained the lowest amount of melt at 18-20%. The distribution of melting extent for the 1.2 GPa experiments is shown in Figure 7 and examined further in the discussion below.

*Phase Equilibria – Depleted Composition*

The two experiments on the depleted mantle composition define phase stability at 1.2 GPa with melt $H_2O$ contents of ~2.5 wt% $H_2O$. At 19% melt and 1240˚C, ol + opx + sp are stable, and at 6% melt and 1225˚C, ol + opx + cpx + sp are present.

## *Assessing Equilibrium*

*KDs, Fe loss/gain, and Textural Evidence*

All experiments included in this study have been assessed for equilibrium using $K_D$s between the minerals and the melt $\left(K_D = \frac{X_{Fe}^{Xstal} * X_{Mg}^{melt}}{X_{Mg}^{Xstal} * X_{Fe}^{melt}}\right)$, variation in bulk composition, and textural evidence of compositionally homogeneous crystals. Experiments were deemed successful if the olivine-melt $K_D$ was between 0.29 and 0.36. Experiments outside of this range exhibited significant Fe loss (greater than 12%, increase in $K_D$) or substantial quench crystal growth (decrease in $K_D$). Of the successful runs, 14 of the 19 runs lost or gained less than 5% Fe. Equilibrium conditions were further established using textural evidence of homogenous crystals and glass in the run products (Figure 3). $K_D$s and Fe loss/gain are reported in Table 2, and compositions of experimental run products are reported in Table 4.

*$H_2O$*

All hydrous piston cylinder experiments undergo $H_2O$ loss, and the experiments presented in this study are no exception. The experiments presented are considered to be at equilibrium because the amount of water lost ($H_2O$ added – $H_2O$ retained (corrected for melt fraction)) does not increase with run duration. We present hydrous experiments conducted from 8-73 hours, and the amount of $H_2O$ lost decreases with run duration, suggesting that $H_2O$ loss occurs in the first few hours of the run and that $H_2O$ contents measured represent equilibrium values.

*$Na_2O$*

Our experiments incorporated up to two times the $Na_2O$ of the H&Z fertile mantle (Table 1) in an attempt to model the input of alkalis from the subducting slab; however, mass balance calculations for $Na_2O$ show significant differences between the starting values and measured EPMA analyses. A recent investigation by Morgan and London (2005) suggests that the conditions under which our hydrous glasses were analyzed could have caused up to approximately 50% Na loss. This suggests that the difference between our bulk $Na_2O$ and the $Na_2O$ of our experimental products is caused by low measurements of glass $Na_2O$ during EPMA analysis. Because there is no significant $Na_2O$ loss from the sealed Pt capsules, the value of $Na_2O$ in the glass is corrected using phase proportions from the LIME program (Krawczynski and Olive 2011) in conjunction with measured $Na_2O$ values for the solid phases. These corrected values are included in Table 4 and are used in the discussion as the amount of $Na_2O$ in glass.

## *Discussion*

### *Quantitative Model of the Olivine-Orthopyroxene Saturation Boundary*

#### *Experiments Used to Calibrate Model*

The empirical, quantitative model presented is calibrated using experimental data from this study as well as from other experimental studies that were found using the Library of Experimental Phase Relations (Hirschmann et al. 2008; Table 5). All experiments contain melt in equilibrium with ol + opx ± sp. Experiments included were conducted between 1 and 2.5 GPa, the pressure range of interest for water-undersaturated mantle wedge melting. Experiments used for calibration were restricted to those studies that contained at least one $H_2O$-bearing experiment. This requirement was imposed because the goal of the modeling was to investigate the influence of $H_2O$, and the intent was to develop a model dataset that was not dominated by anhydrous glass compositions. The calibration dataset did not include four experiments that fit the requirements described above (B408, Gaetani and Grove (1998); D86, D88, and B859, Hesse and Grove (2003)). These four runs were excluded because high $K_2O$ and low $SiO_2$ contents of the glasses caused these experiments to plot in silica undersaturated space in the Tormey pseudo-ternary projection schemes (Tormey et al. 1987).

*Thermodynamic Foundation for the Model*

The melting model developed here uses the approach of Kinzler and Grove (1992; hereafter KG92), Kinzler (1997), and Till et al. (2012a). It represents an adaptation of the Gibbs method (Spear et al. 1982) in which three sets of constraints describe the melting equilibrium: (1) mass balance (constraining the system's bulk composition), (2) stoichiometry (constraints from the compositions of the reacting phases), and (3) thermodynamic equilibrium.

In KG92, the constraint of thermodynamic equilibrium (constraint 3) is represented by a melting reaction between solid and liquid phases, where the composition of the melt in equilibrium with either spinel- or plagioclase-lherzolite is predicted in terms of mineral components and is based on the composition of the solid phases. By specifying a sufficient number of compositional and intensive variables, KG92 calculates the melts of a natural mantle

peridotite system over a range of pressure, temperature, and composition space. The models in this study follow the methods of KG92 and represent the constraint of thermodynamic equilibrium using compositional and intensive variables to predict the composition of mantle melts in equilibrium with spinel harzburgite or lherzolite over a range of pressure, temperature, composition space, and $H_2O$ content.

The thermodynamic variance of the melting equilibrium can be inferred using the Gibbs Phase Rule, which states that the variance (degrees of freedom, F) of the system equals the number of components C plus the number of intensive variables (in this case, Temperature and Pressure) minus the number of phases Φ (Equation 1).

$$F = C + 2 - \Phi \quad (1)$$

In the simple mantle analogue system, CMAS, there are only four components (CaO, MgO, $Al_2O_3$, and $SiO_2$) in addition to the two intensive parameters temperature and pressure. At the multiple saturation point, lherzolite melting experiments contain 5 phases: melt, ol, opx, cpx, and an Al-phase (plagioclase or spinel). Using Equation 1, the variance of the CMAS system at the multiple saturation point is univariant (F = 1). When F=1, fixing one variable determines the other variables in the system (i.e. fixing pressure determines the temperature and composition of the melt at equilibrium).

Unlike CMAS, natural systems involve additional chemical components ($TiO_2$, $Cr_2O_3$, FeO, $K_2O$, $Na_2O$, and $H_2O$); the model presented in this study includes ten of these compositional components recast as phase components and exchange components following KG92. For spinel harzburgite melting, the focus of this study, 4 phases are present and Φ=4. Thus, the Gibbs Phase Rule (Equation 1) dictates that F = 10 + 2 – 4 = 8. If spinel is absent, Φ=3, and F = 9. This means that there are 8 and 9 degrees of freedom for the system, respectively. Of

the 8 or 9 degrees of freedom, two degrees of freedom are attributed to the temperature and pressure, and the remaining 6-7 degrees of freedom are attributed to the compositional components.

Contrary to the CMAS example above, in our models, eight or nine variables must be fixed and are chosen as predictors (pressure and compositional components) in order to determine outcomes (temperature and compositional components) using multiple linear regressions. Our model determines the best possible combination of the predictors using Akaike Information Criteria (discussed below; Akaike 1974). Since some of the compositional predictors do not increase the precision of the prediction, these predictors are not included in the final equations presented, making it possible for the equations to contain fewer than eight or nine predictor variables. In the model presented here, the initial predictors for the compositional endmember and temperature predictions are Pressure, 1-Mg# $\left(1-\left(\frac{X_{Mg}}{X_{Mg}+X_{Fe}}\right)\right)$ (molar units), NaK# $\left(\frac{Na_2O+K_2O}{Na_2O+K_2O+CaO}\right)$ (wt% units), $H_2O$, $TiO_2$, and $Cr_2O_3$, (wt%) where a few of the predictors are combined into single parameters, following KG92 (i.e. $Na_2O$, $K_2O$, and CaO are three variables represented by the single variable NaK#). Of the twelve components, these initial predictors were chosen because 1) previous work has shown that Pressure, 1-Mg#, and NaK# exercise systematic influence on the compositions of multiply saturated liquids in mantle lherzolite melting models, 2) 1-Mg# and NaK# characterize or represent solid solutions in the heterogeneous reactions calculated, and 3) for applications of the model, these are values that can be obtained using partition coefficients, stoichiometry, and mass balance. The outcomes calculated are predicted melt compositions expressed in mineral components $CaMgSi_2O_6$ +

$CaFeSi_2O_6$ (Cpx), $Mg_2SiO_4 + Fe_2SiO_4$ (Ol), $CaAl_2Si_2O_8 + NaAlSi_3O_8$ (Plag), and $SiO_2$ (Qz) as described by Tormey et al. (1987) (expressions corrected in Grove 1993) and temperature.

The initial predictors for pressure are 1-Mg#, NaK#, $H_2O$, $TiO_2$, $Cr_2O_3$, Cpx, Ol, and Plag, and the initial predictors for $H_2O$ are Pressure, 1-Mg#, NaK#, $TiO_2$, $Cr_2O_3$, Ol, Plag, and Qz. The predictors chosen for the Pressure and $H_2O$ regressions are different from Cpx, Ol, Plag, Qz, and Temperature because the compositional endmembers and temperature use pressure and $H_2O$ as predictors. Only three of four compositional endmembers are used in the Pressure and $H_2O$ regressions in order to retain linear independence and prevent rank deficiency.

*Modeling Methods*

The model presented in Table 6 uses Akaike Information Criteria (AIC) (Akaike 1974) to determine the best combination of predictor variables through consideration of both goodness of fit and the complexity of the model. For the compositional regressions presented, it was determined that an identical set of predictor variables produced almost indistinguishable results compared to a model with unique predictor variables for each regression. Model recovery of experimental data is shown in Figure 4. Detailed modelling methods are included in the Modelling Methods Online Supplementary Material.

*Model Comparison*

The thermobarometer presented in this paper is compared to the thermobarometer presented in Lee et al. (2009) as well as the barometers presented in Wood and Turner (2009) (Figure 5). While it would be ideal to test the models using experiments not included in the calibration, this is not possible given the limited amount of hydrous experimental data. Model calculations for this study and Lee et al. (2009) are performed on the experimental data used to calibrate the model in this study. Of the experiments used to test the models, 48 experiments are also used to calibrate the Lee et al. (2009) model. Model calculations for the

Wood and Turner (2009) barometers are performed using the experimental data presented in this study.

In both temperature and pressure, our model predicts the experimental temperature and pressure more accurately than both Lee et al. (2009) and Wood and Turner (2009) (Figure 5). In temperature, the Lee et al. (2009) thermometer has a mean average error (mae) of 84 °C and predicts lower temperatures than the experimental temperatures, especially at higher experimental temperatures. Our model reproduces experimental temperatures equally well at low and high experimental temperatures and has a mae of 23 °C using the barometer presented in this study. In pressure, the Lee et al. (2009) model has a mae of 0.59 GPa and predicts lower pressures than the experimental values. The Wood and Turner (2009) barometer has a mae of 0.56 GPa and over predicts the experimental pressures, such that their model predicts pressures of up to 3.1 GPa for experiments conducted at 2 GPa. The barometer presented in this study, however, is able to predict the experimental pressures with increased and more consistent accuracy throughout the calibrated range of 1-2.5 GPa with a mae of 0.14 GPa.

*Systematics of the Experimental Results*

The experiments presented in this paper comprise the first comprehensive investigation of the melting behavior of ol + opx ± sp bearing fertile mantle composition as a function of variable pressure and water content.

*Role of Pressure on Fertile Melt Composition*

To understand the role of pressure on melt composition, four experiments at variable pressure with similar melt extents and $H_2O$ contents are examined (Figure 6). Results from these water-undersaturated experiments are consistent with experimental studies conducted on both anhydrous (Kushiro 1996; Walter 1998) and water-saturated mantle peridotite (Grove et al. 2006, Till et al. 2012b). Under anhydrous and $H_2O$-bearing conditions, melt compositions become

more olivine-normative as pressure increases. This is quantified in the model presented, which shows that per 1 GPa increase, the Ol component increases by 0.111 as the Plag and Qz components decrease by 0.0612 and 0.0807. This parameterization of pressure is broadly consistent with previous modeling formulations, such as the spinel lherzolite model of Till et al. (2012a). In both models, coefficients for Cpx and Ol are positive, and coefficients for Plag and Qz are negative, though the magnitude of the coefficients is slightly different between the model formulations (Ol: 0.111 (this study) versus Ol: 0.085 (Till et al. (2012a)).

*Role of Extent of Melting on Fertile Melt Composition*

Figure 7 compares the variable $H_2O$, 1.2 GPa experiments of this study with the anhydrous mantle melting experiments of Baker and Stolper (1994) and Baker et al. (1995). Baker and Stolper (1994) and Baker et al. (1995) found that melt compositions move away from the plagioclase component as degree of melting increases. This trend is also apparent in the experiments of Hirose and Kawamoto (1995) as well as in our 1.2 GPa experiments on the FM composition. In the higher $H_2O$ experiments of this study (Figure 7: circles that form a vertical trend closer to the quartz component), the experiments move directly away from plagioclase with increases in melt extent from 29%→32%→38%→39%→ 44% melt. The composition of glasses in experiments with lower $H_2O$ also move away from plagioclase with increasing melt extent, showing that regardless of the horizontal scatter of the data from this study (caused by changes in $H_2O$ content), increasing extent of melting has the same effect on melt composition.

*Role of $H_2O$ on Fertile Melt Composition*

Since the early work of Kushiro et al. (1968) and Kushiro (1969, 1970, 1972, and 1974), it has been known that as $H_2O$ content increases, melt compositions become increasingly quartz normative. This effect is seen in the experiments presented here (Figure 8) and is quantified for

the first time. With an increase of 1 wt% $H_2O$, the Qz component increases by 0.00840 while Cpx and Ol decrease by 0.00660 and 0.00320 and Plag increases by 0.00140.

Our results are consistent with other mantle melting studies, such as the dry 1 GPa experiments of Baker and Stolper (1994; Figure 8) and the wet 1 GPa experiments of Hirose and Kawamoto (1995) and Hirose (1997). The similarity of the Hirose and Kawamoto (1995) glass compositions to the Baker and Stolper (1994) glasses indicates that the majority of the Hirose and Kawamoto (1995) data are dry. It is possible that they are dry because Hirose and Kawamoto (1995) only measured $H_2O$ for three experiments, and the measured $H_2O$ values of these three experiments differed by up to 50% from their calculated values. The two $H_2O$-bearing runs of Hirose and Kawamoto (1995) and the higher $H_2O$ content experiments of Hirose (1997) add further support to the observation that $H_2O$ drives melt compositions to be more quartz normative.

*Primitive Mantle Melts and Primitive High-Mg#, High-MgO Basaltic Andesites & Andesites*

This study aims to understand whether the process of isobaric melting can produce high-Mg#, high-MgO basaltic andesites and andesites (primitive andesites—PA). PA are a subset of primitive, high Mg# andesites (HMA) as defined by Kelemen (1995). In this study, we selected primitive basaltic andesite and andesite lavas that have both high Mg# and high MgO. Natural samples are from four locations–Kamchatka, Cascades, Setouchi, and Mexico. The following chemical characteristics were used to select the lavas shown in Figure 9: Mg# $\geq$ 0.70, $SiO_2 \geq 51$ wt%, MgO$\geq$7 wt%, $TiO_2 \geq 0.4$ wt%, $K_2O \leq 3$ wt%. $TiO_2$ bounds were chosen to exclude boninite compositions, and $K_2O$ bounds were chosen to remove shoshonitic rocks from the Argentine Puna plateau (Kay et al. 1994) from consideration. The restriction to high MgO values is imposed because we do not apply a correction for fractionation for the lavas. However, we do

consider a suite of glassy and microcrystalline quenched magmatic inclusions corrected to primitive compositions from Mt. Shasta, CA (Krawczynski 2011). For the Kamchatka, Cascades, and Setouchi samples, the major elements $SiO_2$, FeO, CaO, $K_2O$ and $Na_2O$, define distinct trends (Figure 9). The corrected quenched inclusions from Mt. Shasta bridge the compositional gaps between the lava trends from the three arcs (Figure 9, 10), indicating that the range of compositions from the three locations can be formed at a single volcanic system.

The following mechanisms have been proposed to explain the petrogenesis of HMA: 1) direct, hydrous partial melting of the mantle (Kushiro 1969, 1972, 1974; Baker et al. 1994; Grove et al. 2002; Grove et al. 2003), 2) mixing of primitive basaltic and dacitic magmas (Straub et al. 2008; Straub et al. 2011), and 3) partial melting of subducted oceanic crust followed by assimilation of peridotite within the mantle wedge (Kay 1978; Kelemen et al. 2003; Bryant et al. 2010). In the following section, the viability of each of these mechanisms will be explored in the context of PAs from the Cascades, Kamchatka, Setouchi, and Mexico (Grove et al. 2002; Barr 2010; Bryant et al. 2010; Tatsumi and Ishizaka 1982; Weaver et al. 2011; and Weber et al. 2011).

*Mechanism 1: Direct Mantle Melting*

Tatsumi's (1981) inverse experimental study on the Teraga-Ike (TGI) PA from Setouchi showed that, when water-saturated, TGI is in equilibrium with olivine and orthopyroxene at 1.55 GPa, 1080˚C, or, when water-undersaturated, TGI is in equilibrium with a harzburgite residue at lower pressures and higher temperatures. Later, Baker et al. (1994) showed that the high-MgO basaltic andesites and andesites from the Cascades (Mt. Shasta) are in equilibrium with olivine and orthopyroxene at 1.0 GPa, with 3-6% $H_2O$. Two more recent studies on lavas from the Trans-Mexico Volcanic Belt have also determined conditions at which PA lavas were in equilibrium with ol and opx: d-25 at >7 wt% $H_2O$ and 1.1-1.5 GPa (Weber et al. 2011) and JR-

28 at 5-6 wt% $H_2O$ and 1.2-1.4 GPa (Weaver et al. 2011). We can now compare these inverse studies with our new forward model.

When model results are compared to the compositions of the lavas from Kamchatka, the Cascades, Setouchi, and Mexico (Figure 10), pressure and $H_2O$ contents can be determined. For the majority of the natural samples, neither pressure of last equilibration nor pre-eruptive water content is known, so model estimates must fix one the two variables in order to determine the other (i.e. fixing pressure at 1.5 GPa would give a $H_2O$ content of 7 wt%). For Cascades lava 85-44, however, the pressure at which the melt was in equilibrium with ol+opx was determined in the experimental study of Baker et al. (1994) to be 1.0 GPa. Using a pressure of 1.0 GPa, the model returned a $H_2O$ content of 4.3 wt% for 85-44, which is in the middle of the 3-6 wt% $H_2O$ range provided by Baker et al. (1994). Experimental studies have also been conducted on two lavas from the Trans-Mexico Volcanic Belt: d-25 (Weber et al. 2011) and JR-28 (Weaver at al. 2011). Weber et al. (2011) found that d-25 equilibrated with >7 wt% $H_2O$ at 1.1-1.5 GPa. Our model predicts that at 1.0 and 1.5 GPa, lava d-25 equilibrated with 5.2 and 7.8 wt% $H_2O$, respectively. In the second lava from the Trans-Mexico Volcanic Belt, Weaver et al. (2011) found that JR-28 equilibrated with a harzburgitic residue at 5-7 wt% $H_2O$ and 1.2-1.4 GPa. JR-28 is predicted by our model to equilibrate with 4.8 and 7.4 wt% $H_2O$ at 1.0 and 1.5 GPa. For all three natural lavas with experimental $H_2O$ determinations, the model presented here successfully predicts $H_2O$ contents.

Crustal thickness estimates for each locality provide a limit for the shallowest pressure of equilibration in the mantle. Crustal thickness models suggest a depth of 37 km at the sample locality of Shisheika Volcano in Kamchatka (Iwasaki et al. 2013; Baboshina et al. 1984) and a depth of 34-38 km at Mount Shasta in the Cascades (Zucca et al. 1986; Ritter and Evans 1997;

and Mooney and Weaver 1989). In Mexico, crustal thickness below the Pelagatos cinder cone of the Chichinautzin Volcanic Field (d-25) is ~40 km (Pérez-Campos et al. 2008), and crustal thickness is >35 km below the Michioacán-Guanajuato Volcanic Field (JR-28; Guilbaud et al. 2011; Gómez-Tuena et al. 2007). Using an average crustal density of 2750 kg/m$^3$, the pressures associated with these depths are 1.0 GPa (Kamchatka), 0.9-1.0 GPa (Cascades), and 0.9, 1.1 GPa (Mexico). Consistent with these crustal thicknesses, the model predicts a lower limit of 1.0 GPa for the majority of the Kamchatka and Cascades lavas and both Mexican lavas regardless of the amount of $H_2O$. If pressure is fixed in the model at 1.0 GPa, then the Kamchatka, Cascades, and Mexican samples span a range of $H_2O$ contents from 3.2 to 5.6 wt% (Table 7). These $H_2O$ predictions, in addition to $H_2O$ predictions for Setouchi support the observation that increasing $H_2O$ makes melts more quartz-normative, raising $SiO_2$ contents (Figure 11).

The Setouchi lavas were erupted 13.7±1.0 (1σ) Ma (Tatsumi 2006). To provide a limit on the pressure of last equilibration, we have used a modern crustal thickness in southwest Japan of approximately 30 km (Yoshii et al. 1974; Ito et al. 2009). This depth corresponds to 0.8 GPa using an average crustal density of 2750 km/m$^3$. At this minimum pressure, the model results predict that the Setouchi samples contain 1.9-6.1 wt% $H_2O$. For all natural samples considered, particularly the Setouchi lavas, the predicted movement of the ol-opx saturation boundary with increasing $H_2O$ content is parallel to sample trends in both Ol-Cpx-Qz and Ol-Plag-Qz pseudoternary space (the $H_2O$ vectors in Figure 10), indicating the significant control that variation in water content has on the compositional variation of the lavas from each arc.

The experimental results of this and other studies suggest a maximum range of 20-30% for the degrees of melting under which natural PAs formed. The inverse experimental results from Tatsumi (1981), Baker et al. (1994), Weaver et al. (2011), and Weber et al. (2011) indicate

that the natural PAs are in equilibrium with olivine and orthopyroxene. In order to be in equilibrium with a harzburgitic residue, the system must melt past the point of cpx-out, which is achieved at higher degrees of melting or after prior episodes of melt extraction. When natural samples are projected through Cpx onto the Ol-Plag-Qz pseudoternary, they plot away from Plag, at approximately F=0.2-0.3, as defined by 1.0 GPa experiments from this study as well as Baker et al. (1995) and Baker and Stolper (1994). Therefore, the natural lavas are either melts of the fertile mantle having undergone extents of melting of 0.2-0.3 or they are melts of the previously depleted mantle at lower extents of melting. Experiment C548, one of the two depleted runs in this study that contains 19% melt plots at the same location in the Ol-Plag-Qz pseudoternary as our fertile experiments that contain 29% melt. It is thus possible that if the mantle were depleted to the extent of our model depleted composition, then the natural PAs could have been formed at F=0.1-0.2. Since the amount of prior depletion is unknown, the maximum amount of melting for the PAs is given by the fertile composition at F=0.2-0.3.

At pressures of at least 1.0 GPa, melt fractions of at most 0.2-0.3, and variable amounts of $H_2O$, the compositions of the experiments reproduce the range of natural lavas in $SiO_2$, $TiO_2$, $Al_2O_3$, MgO, and $Na_2O$. At 4-6 wt% $H_2O$ and in equilibrium with a harzburgitic residue, the experimentally-produced direct mantle melts have both high $SiO_2$ and high Mg#. As the combination of high $SiO_2$ and high MgO in the natural PAs is anomalous, producing experimental glasses with this unique chemistry in equilibrium with a harzburgitic residue (as suggested by inverse experiments on HMA) suggests that direct mantle melting is a viable mechanism for producing many of the major element characteristics of PAs.

The major elements FeO, CaO, $K_2O$ in our experimental glasses do not always correspond directly to the range defined by the natural lavas (Figure 9). In our experimental bulk

compositions, the amounts of $K_2O$ and $Na_2O$ are greater than is estimated for fertile and depleted mantle compositions to account for the introduction of alkalis from the subducting slab. Since the amount of $K_2O$ added was an estimated slab contribution, the discrepancy between the experimental glass compositions and the natural PAs indicates that more $K_2O$ is being added to the mantle wedge in the natural system than assumed in creating the starting materials for this study. Thus, the amount of $K_2O$ in our starting material provides a lower bound on the amount being added to the slab (Figure 9).

At a given MgO content, the experimentally produced fertile mantle glass compositions have higher CaO contents than the natural samples by 1-5 wt%. Based on the initial experimental results from this study, three hypotheses were investigated to account for this disparity. First, the conditions of the experimental runs were changed to increase the extent of melt at higher $H_2O$ contents for melts in equilibrium with a harzburgitic residue. Results from this hypothesis (C553: *F=0.39(3), $H_2O$=5.9(4) wt%*; C554: *F=0.38(2), $H_2O$=4.7(2) wt%*) determined that the CaO contents under such conditions would be lower than our initial glass compositions (8.3, 8.6 wt% compared to previous values of 10-11 wt% CaO). As expected, the $Al_2O_3$ contents of these experiments were also lower (10.9, 11.7 wt%), dropping out of the range of the natural PAs (13.6-16.9 wt%). With such high extents of melting, the MgO contents of the glasses were also significantly higher than the natural PAs (~14.5 wt% compared to 7.5–12 wt%). Thus, high extents of melting with high $H_2O$ contents successfully lowered the CaO content but also caused the concentrations of MgO and $Al_2O_3$ to diverge from the natural samples, suggesting that these conditions do not contribute to the production of PAs.

The second hypothesis was to change the starting material to a more depleted composition, which by definition contains less CaO, to determine whether a change in the

composition of the source could account for the differences seen in CaO. Two experiments were conducted on the depleted composition: experiment C548 contained gl+ol+opx+sp, and experiment C544 contained gl+ol+opx+cpx+sp (black stars, Figure 9). The experiment with the harzburgitic residue (C548) contained less CaO than the fertile experiments at a similar MgO content but only by 0.5-1 wt% CaO. This is not a significant enough difference to produce the very low CaO contents of the natural lavas, which extend 1–5 wt% CaO below the fertile experiments. Experiment C544 was a very low degree melt (6%) in equilibrium with cpx. Because cpx was present in the residue, the amount of CaO in the glass is very low and does reproduce the lowest range of the natural PAs. However, the natural lavas are not in equilibrium with cpx, so this low degree melt does not explain the low CaO contents in the natural samples.

Based on the results from the FM experiments in this study and the depleted experiments of Wasylenki et al. (2003), the CaO content of melt in equilibrium with a harzburgitic residue will either remain constant or increase with decreasing MgO content. If this holds true for the DM experiments, then after cpx-in, the CaO content of the melt must decline rapidly with smaller decreases in MgO until the composition produced in C544 is reached. Once this predicted change in slope occurs, the melts will no longer be in equilibrium with a harzburgitic residue, which is a requirement of the natural PAs. Therefore, predicted melting paths between the two DM experiments in CaO v. MgO space are limited to paths with two segments—a shallower component followed by a steeper one as MgO content decreases. Even if cpx out were just below the MgO content of C548 (at a slightly lower value than 11.6 wt% MgO), the CaO contents of the melting path would be limited by a line connecting the two melt compositions. It would not be possible for the melting path to be concave up between the two DM runs based on the results of Wasylenki et al. (2003) and this study that show CaO remains constant or increases

as MgO decreases for melts in equilibrium with a harzburgite residue. In other words, the first segment of the melting path must have a negative slope or zero slope (Figure 9). Example estimated paths above this line are plotted in Figure 9. The majority of the range of PAs is not included in this region of CaO v. MgO space, making melting a more depleted mantle composition an unlikely solution for producing the low CaO of the natural PAs.

The third hypothesis to account for the low, location-dependent CaO contents in the natural PAs is reaction between melts generated deeper in the mantle wedge and melts at 1.0-1.2 GPa. Experimental glasses generated at 3.2 GPa have very low Ca contents, as seen by the glass composition measured in the $H_2O$-saturated experiment D206 of Till et al. (2012b), which has 1.92±1.29 wt% CaO. This experiment was conducted on a fertile mantle lherzolite composition at the conditions of the onset of melting at subduction zones. It is unrealistic to model the direct mixing of a deep melt such as D206 with the glasses produced in this study because the changes to such a melt as it rises through the melting column are dynamic and beyond the scope of this discussion. Thus, we suggest but do not quantify that the low CaO contents of the PAs are caused or at least influenced by these deep, low CaO mantle melts.

*Mechanism 2: Mixing Primitive Basaltic and Dacitic Magmas*

Straub et al. (2008) and Straub et al. (2011) reason that primitive, high-Mg# andesites found in the Central Mexico Volcanic Belt (CMVB) are a consequence of mixing between primitive basaltic and dacitic magmas based on moderately high Ni contents of olivine (700-1000 ppm Ni) in equilibrium with low MgO melt compositions (2-8 wt% MgO). The two Mexican samples considered here, however, contain higher MgO contents at 9.38 wt% (d-25) and 9.43 (JR-28) wt%, suggesting that these samples were partial melts of peridotite and not the result of mixing between primitive basalt and dacite magmas. In the Cascades PAs, olivine phenocrysts with $Fo_{93.8}$ contain high Ni contents (2300 ppm (85-41c), 3000 ppm (07-28)) that are

in equilibrium with high MgO melt compositions (9.14 wt% MgO; 10.03 wt%, respectively) (Baker et al. 1994; Barr 2010). If these samples are plotted on Ni wt% v. Fo mole% (Figure 9, Straub et al. 2008), then they fall into the range of partial melts of peridotite, as defined by Straub et al. (2008). Chemical characteristics similar to that of the Cascades samples define the Setouchi samples: high Ni contents (≥3100 ppm) in high-Fo olivine in equilibrium with high melt MgO (7.59-10.34 wt%) (Tatsumi and Ishizaka 1982). The CMVB lavas of Straub et al. (2008, 2011) do not plot in the range of partial melts of peridotite as the Cascades and Setouchi samples do, so while mixing of primitive basaltic and dacitic melts is viable for many of the CMVB samples, the petrogenetic histories for the Cascades and Setouchi samples are different.

Though the Kamchatka lavas plot outside of the range of primitive mantle melts in Figure 9 of Straub et al. (2008), Bryant et al. (2010) rejected the hypothesis that mixing primitive basaltic and dacitic magmas could explain the petrogenetic history of the Kamchatka PAs. The high whole rock Ni/MgO ratios (20 ppm/wt%) of the Kamchatka lavas cannot form by mixing of relatively high Ni/MgO (10-20 ppm/wt%) of primitive basalts and low Ni/MgO (2-7 ppm/wt%) of dacites. Thus, the petrogenetic history of lavas from Kamchatka, Setouchi, and the Cascades does not appear to involve mixing of primitive dacites and basalts, as is suggested for HMAs from the Central Mexico Volcanic Belt.

*Mechanism 3: Melting Subducted Oceanic Crust, then Assimilation of Overlying Mantle*

Kelemen et al. (2003) use trace element systematics to suggest that enriched, primitive Aleutian andesites formed as a result of partial melting of eclogite, followed by reaction with the overlying mantle wedge. The models presented by Kelemen et al. (2003) are a quantification of the long-standing realization that partial melting of subducting material supplies a component that carries incompatible elements and alkalis into the mantle wedge. The process whereby this component is added to the overlying mantle and the incorporation of these elements during the

initiation of flux melting of the metasomatized base of the mantle wedge is beyond the scope of this experimental study. However, the trace elements in PA lavas are consistent with the Kelemen et al. (2003) hypothesis that melts formed in subducting oceanic crust and/or sediment in eclogite facies contribute to flux melting in the mantle wedge. It is also clear that the element addition and incorporation in the mantle melt must be a complex multi-stage process. Other simple mass balance estimates of the slab-derived components added to form subduction zone melts (Stolper and Newman, 1994; Grove et al., 2002) conclude that most (> 90 %) of the incompatible trace elements as well as light and middle rare earth elements are contributed from a slab component and that $Na_2O$ and $K_2O$ appear to be present as major elements and constitute nearly 30 wt. % of the "fluid-added" component. Thus, while we acknowledge the addition of a slab melt to form arc magmas, the specific process through which it occurred has yet to be resolved.

## *Conclusions*

This study quantitatively assesses the influence of pressure, extent of melting, and $H_2O$ on melt compositions of a fertile mantle lherzolite plus a metasomatic slab component at $H_2O$-undersaturated conditions. Melts are produced that contain high $SiO_2$ (55-57 wt%) at high MgO ($\geq$8 wt%). In addition, it is determined that natural high Mg#, high MgO basaltic andesites and andesites (PAs) from Kamchatka, the Cascades, Setouchi, and Mexico are likely produced at variable pressure (1.0-1.5 GPa), extent of melt (F=0.2-0.3), and $H_2O$ content (~3-9 wt%).

## *Acknowledgements*

The authors would like to thank Bernard Charlier for his guidance early on in the laboratory, Neel Chatterjee for assistance with the electron microprobe, Brian Monteleone for his help with the ion microprobe, as well as Lisa Miller and Randy Smith for their assistance using

the U2B beamline at the National Synchrotron Light Source. Many thanks Oliver Jagoutz for his thoughtful suggestions and help testing the excel spreadsheet, as well as Benjamin Mandler, Stephanie Brown, and Max Collinet for their insights during our many discussions. In addition, the authors would like to thank Peter Kelemen and an anonymous reviewer for their thoughtful comments and suggestions, as well as Othmar Müntener for his remarks and editorial handling of the manuscript. The work in this manuscript was supported by the National Science Foundation EAR-1118598 granted to Timothy L. Grove. Use of the National Synchrotron Light Source, Brookhaven National Laboratory, was supported by the U.S. Department of Energy, Office of Science, Office of Basic Energy Sciences, under Contract No. DE-AC02-98CH10886.

## *Supplemental Material*

**1. Experimental Methods**

**2. Analytical Methods**

**3. Modelling Methods**

**4. Model in Excel**

An excel spreadsheet is included in online supplemental materials to aid with use of the model presented. The spreadsheet calculates the first three equations in Table 6 using two methods: it calculates 1) P (GPa) and T (°C) of last equilibration for known $H_2O$ contents of last equilibration or 2) $H_2O$ (wt%) and T (°C) of last equilibration when the Pressure (GPa) of last equilibration is known. To use the spreadsheet, enter your compositions into the 'Input' sheet as well as your known $H_2O$ or Pressure for each composition. The sheet goes through the following steps:

1) renormalizes the compositions

2) converts compositions to molar values

3) converts all oxides to single cation units

4) converts to single oxygen units

5) calculates the Cpx, Ol, Plag, Qz endmembers of Tormey et al. (1987) (corrected in Grove 1993)

6) calculates P and T or $H_2O$ and T using the equations in Table 6.

The results of each step are outputted in the 'Calculations' sheet. Final values are reported in the 'Output' sheet. Sample names are automatically copied across each sheet for easy analysis of results.

## *References*


Akaike, H. (1974). A new look at the statistical model identification. *Automatic Control, IEEE Transactions on*, *19*(6), 716-723.

Armstrong, J. T. (1995) CITZAF: A package of correction programs for the quantitative electron microbeam X-ray analysis of thick polished materials, thin films, and particles. *Microbeam Analysis-Deerfield Beach*, *4*, 177-200.

Baboshina, V. A., Tereschenkov, A. A., Kharakhinov, V. V. (1984). Deep structure of the Sea of Okhotsk according to geophysical data, overview information. *Vsesouzniy Nauchno-Issledovatelskiy Institute (VNII) Gazprom*, *3*, 41.

Baker, M. B., Grove, T. L., Price, R. (1994) Primitive basalts and andesites from the Mt. Shasta region, N. California: products of varying melt fraction and water content. *Contributions to Mineralogy and Petrology*, *118*(2), 111-129.

Baker, M. B., Hirschmann, M. M., Ghiorso, M. S., Stolper, E. M. (1995) Compositions of near-solidus peridotite melts from experiments and thermodynamic calculation. *Nature*, *375*(6529), 308-311.

Baker, M. B., Stolper, E. M. (1994) Determining the composition of high-pressure mantle melts using diamond aggregates. *Geochimica et Cosmochimica Acta*, *58*(13), 2811-2827.

Barr, J.A. (2010) Primitive Magmas of the Earth and Moon: A Petrologic Investigation of Magma Genesis and Evolution. Dissertation, Massachusetts Institute of Technology.

Boyd, F. R., England, J. L. (1960) Apparatus for phase-equilibrium measurements at pressures up to 50 kilobars and temperatures up to 1750 C. *Journal of Geophysical Research*, *65*(2), 741-748.

Bryant, J. A., Yogodzinski, G. M., Churikova, T. G. (2010) High-Mg# andesitic lavas of the Shisheisky Complex, Northern Kamchatka: implications for primitive calc-alkaline magmatism. *Contributions to Mineralogy and Petrology*, *161*(5), 791-810.

Cottrell, E., Kelley, K. A. (2011). The oxidation state of Fe in MORB glasses and the oxygen fugacity of the upper mantle. *Earth and Planetary Science Letters*, *305*(3), 270-282.

Falloon, T. J., Danyushevsky, L. V. (2000). Melting of refractory mantle at 1· 5, 2 and 2· 5 GPa under anhydrous and H2O-undersaturated conditions: implications for the petrogenesis of high-Ca boninites and the influence of subduction components on mantle melting. *Journal of Petrology*, *41*(2), 257-283.

Gaetani, G. A., Grove, T. L. (1998). The influence of water on melting of mantle peridotite. *Contributions to Mineralogy and Petrology*, *131*(4), 323-346.

Gómez-Tuena, A., Orozco-Esquivel, M. T., Ferrari, L. (2007). Igneous petrogenesis of the Trans-Mexican volcanic belt. *Geological Society of America Special Papers*, *422*, 129-181.

Green, D. H. (1973). Experimental melting studies on a model upper mantle composition at high pressure under water-saturated and water-undersaturated conditions. *Earth and Planetary Science Letters*, *19*(1), 37-53.

Grove, T. L. (1993). Corrections to expressions for calculating mineral components in "Origin of calc-alkaline series lavas at medicine lake volcano by fractionation, assimilation and mixing" and "Experimental petrology of normal MORB near the kane fracture zone: 22°-25° N, mid-atlantic ridge". *Contributions to Mineralogy and Petrology*, *114*(3), 422-424.

Grove, T. L., Chatterjee, N., Parman, S. W., Médard, E. (2006). The influence of $H_2O$ on mantle wedge melting. *Earth and Planetary Science Letters*, *249*(1), 74-89.

Grove, T. L., Elkins-Tanton, L. T., Parman, S. W., Chatterjee, N., Müntener, O., Gaetani, G. A. (2003). Fractional crystallization and mantle-melting controls on calc-alkaline differentiation trends. *Contributions to Mineralogy and Petrology*, *145*(5), 515-533.

Grove, T. L., Juster, T. C. (1989). Experimental investigations of low-Ca pyroxene stability and olivine-pyroxene-liquid equilibria at 1-atm in natural basaltic and andesitic liquids. *Contributions to Mineralogy and Petrology*, *103*(3), 287-305.

Grove, T., Parman, S., Bowring, S., Price, R., Baker, M. (2002). The role of an H2O-rich fluid component in the generation of primitive basaltic andesites and andesites from the Mt. Shasta region, N California. *Contributions to Mineralogy and Petrology*, *142*(4), 375-396.

Guilhaumou, N., Dumas, P. Carr, G.L., Williams, G.P. (1998). Synchrotron infrared microspectrometry applied to petrography in micrometer-scale range: fluid chemical analysis and mapping. *Applied Spectroscopy* 52.8: 1029-1034.

Guilbaud, M. N., Siebe, C., Layer, P., Salinas, S., Castro-Govea, R., Garduño-Monroy, V. H., Le Corvec, N. (2011). Geology, geochronology, and tectonic setting of the Jorullo Volcano region, Michoacán, México. *Journal of Volcanology and Geothermal Research*, *201*(1), 97-112.

Hart, S., Zindler, A. (1986). In search of a bulk-Earth composition. *Chemical Geology* 57(3-4), 247-267.

Hays, J. F. (1966). Lime-alumina-silica. *Carnegie Institute Washington Yearbook*, *65*, 234-239.

Herzberg, C. (2004). Geodynamic information in peridotite petrology. *Journal of Petrology*, *45*(12), 2507-2530.

Hesse, M., Grove, T. L. (2003). Absarokites from the western Mexican Volcanic Belt: constraints on mantle wedge conditions. *Contributions to Mineralogy and Petrology*, *146*(1), 10-27.

Hirose, K. (1997). Melting experiments on lherzolite KLB-1 under hydrous conditions and generation of high-magnesian andesitic melts. *Geology*, *25*(1), 42-44.

Hirose, K., Kawamoto, T. (1995). Hydrous partial melting of lherzolite at 1 GPa: The effect of $H_2O$ on the genesis of basaltic magmas. *Earth and Planetary Science Letters*, *133*(3), 463-473.

Hirschmann, M. M., Ghiorso, M. S., Davis, F. A., Gordon, S. M., Mukherjee, S., Grove, T. L., Krawczynski, M., Médard, E., Till, C. B. (2008). Library of Experimental Phase Relations (LEPR): A database and Web portal for experimental magmatic phase equilibria data. *Geochemistry, Geophysics, Geosystems*, *9*(3).

Ito, T., Kojima, Y., Kodaira, S., Sato, H., Kaneda, Y., Iwasaki, T., Ikawa, T. (2009). Crustal structure of southwest Japan, revealed by the integrated seismic experiment Southwest Japan 2002. *Tectonophysics*, *472*(1), 124-134.

Iwasaki, T., Levin, V., Nikulin, A., Iidaka, T. (2013). Constraints on the Moho in Japan and Kamchatka. *Tectonophysics*, *609*, 184-201.

Kay, R. W. (1978). Aleutian magnesian andesites: melts from subducted Pacific Ocean crust. *Journal of Volcanology and Geothermal Research*, *4*(1), 117-132.

Kay, S. M., Coira, B., Viramonte, J. (1994). Young mafic back arc volcanic rocks as indicators of continental lithospheric delamination beneath the Argentine Puna plateau, central Andes. *Journal of Geophysical Research: Solid Earth (1978–2012)*, *99*(B12), 24323-24339.

Kelemen, P. B. (1995). Genesis of high Mg# andesites and the continental crust. *Contributions to Mineralogy and Petrology*, *120*(1), 1-19.

Kelemen, P. B., Hanghøj, K., & Greene, A. R. (2014). One view of the geochemistry of subduction-related magmatic arcs, with an emphasis on primitive andesite and lower crust. *Treatise on Geochemistry (2nd ed.)*, *4*, 749-806.

Kelemen, P. B., Yogodzinski, G. M., Scholl, D. W. (2003). Along-strike variation in the Aleutian island arc: Genesis of high Mg# andesite and implications for continental crust. *Geophysical Monograph Series*, *138*, 223-276.

King, P. L., Larsen, J. F. (2013). A micro-reflectance IR spectroscopy method for analyzing volatile species in basaltic, andesitic, phonolitic, and rhyolitic glasses. *American Mineralogist*, *98*(7), 1162-1171.

Kinzler, R. J. (1997). Melting of mantle peridotite at pressures approaching the spinel to garnet transition: Application to mid-ocean ridge basalt petrogenesis. *Journal of Geophysical Research: Solid Earth (1978–2012)*, *102* (B1), 853-874.

Kinzler, R. J., Grove, T. L. (1992). Primary magmas of mid-ocean ridge basalts 1. Experiments and methods. *Journal of Geophysical Research: Solid Earth (1978–2012)*, *97*(B5), 6885-6906.

Krawczynski, M.J. (2011). Experimental Studies of Melting and Crystallization Processes in Planetary Interiors. Dissertation, Massachusetts Institute of Technology.

Krawczynski, M.J., Olive, J.A. (2011). A new fitting algorithm for petrological mass-balance problems, AGU Fall Meet. Suppl., Abs. V53B-2613.

Kress, V. C., Carmichael, I. S. (1991). The compressibility of silicate liquids containing $Fe_2O_3$ and the effect of composition, temperature, oxygen fugacity and pressure on their redox states. *Contributions to Mineralogy and Petrology*, *108*(1-2), 82-92.

Kushiro, I. (1969). The system forsterite-diopside-silica with and without water at high pressures. *American Journal Science*, *267*, 269-294.

Kushiro, I. (1970). Systems bearing on melting of the upper mantle under hydrous conditions. *Carnegie Inst. Washington Year Book*, *68*, 240.

Kushiro, I. (1972). Effect of water on the composition of magmas formed at high pressures. *Journal of Petrology*, *13*(2), 311-334.

Kushiro, I. (1974). Melting of hydrous upper mantle and possible generation of andesitic magma: an approach from synthetic systems. *Earth and Planetary Science Letters*, *22*(4), 294-299.

Kushiro, I. (1975). On the nature of silicate melt and its significance in magma genesis; regularities in the shift of the liquidus boundaries involving olivine, pyroxene, and silica minerals. *American Journal of Science*, *275*(4), 411-431.

Kushiro, I. (1996). Partial melting of a fertile mantle peridotite at high pressures: an experimental study using aggregates of diamond. *Earth processes: Reading the isotopic code*, 109-122.

Kushiro, I., Syono, Y., Akimoto, S. I. (1968). Melting of a peridotite nodule at high pressures and high water pressures. *Journal of Geophysical Research*, *73*(18), 6023-6029.

Laporte, D., Toplis, M. J., Seyler, M., Devidal, J. L. (2004). A new experimental technique for extracting liquids from peridotite at very low degrees of melting: application to partial melting of depleted peridotite. *Contributions to Mineralogy and Petrology*, *146*(4), 463-484.

Lee, C. T. A., Luffi, P., Plank, T., Dalton, H., Leeman, W. P. (2009). Constraints on the depths and temperatures of basaltic magma generation on Earth and other terrestrial planets using new thermobarometers for mafic magmas. *Earth and Planetary Science Letters*, *279*(1), 20-33.

Longhi, J. (2005). Temporal stability and pressure calibration of barium carbonate and talc/pyrex pressure media in a piston-cylinder apparatus. *American Mineralogist*, *90*(1), 206-218.

Médard, E., McCammon, C. A., Barr, J. A., Grove, T. L. (2008). Oxygen fugacity, temperature reproducibility, and H2O contents of nominally anhydrous piston-cylinder experiments using graphite capsules. *American Mineralogist*, *93* 11-12), 1838-1844.

Meriggi, L., Macías, J. L., Tommasini, S., Capra, L., Conticelli, S. (2008). Heterogeneous magmas of the Quaternary Sierra Chichinautzin volcanic field (central Mexico): the role of an amphibole-bearing mantle and magmatic evolution processes. *Revista Mexicana de Ciencias Geológicas*, *25*(2), 197-216.

Mooney, W. D., Weaver, C. S. (1989). Regional crustal structure and tectonics of the Pacific coastal states; California, Oregon, and Washington. *Geological Society of America Memoirs*, *172*, 129-162.

Morgan, G. B., London, D. (2005). Effect of current density on the electron microprobe analysis of alkali aluminosilicate glasses. *American Mineralogist*, *90*(7), 1131-1138.

Mysen, B. O., Kushiro, I., Nicholls, I. A., Ringwood, A. E. (1974). A possible mantle origin for andesitic magmas: Discussion of a paper by Nicholls and Ringwood. *Earth and Planetary Science Letters*, *21*(3), 221-229.

Nicholls, I. A., Ringwood, A. E. (1972). Production of silica-saturated tholeiitic magmas in island arcs. *Earth and Planetary Science Letters*, *17*(1), 243-246.

Parman, S. W., Grove, T. L. (2004). Harzburgite melting with and without H2O: Experimental data and predictive modeling. *Journal of Geophysical Research*, *109*(B2), B02201.

Pearce, J. A., Peate, D. W. (1995). Tectonic implications of the composition of volcanic arc magmas. *Annual Review of Earth and Planetary Sciences*, *23*, 251-286.

Pérez-Campos, X., Kim, Y., Husker, A., Davis, P. M., Clayton, R. W., Iglesias, A., Pacheco, J.F., Singh, S.K., Manea, V.C., Gurnis, M. (2008). Horizontal subduction and truncation of the Cocos Plate beneath central Mexico. *Geophysical Research Letters*, *35*(18).

Ritter, J. R., Evans, J. R. (1997). Deep structure of Medicine Lake volcano, California. *Tectonophysics*, *275*(1), 221-241.

Sisson, T. W., Grove, T. L. (1993). Experimental investigations of the role of H2O in calc-alkaline differentiation and subduction zone magmatism. *Contributions to Mineralogy and Petrology*, *113*(2), 143-166.

Spear, F. S., Ferry, J. M., Rumble, D. (1982). Analytical formulation of phase equilibria; the Gibbs' method. *Reviews in Mineralogy and Geochemistry*, *10*(1), 105-152.

Stolper, E., Newman, S. (1994). The role of water in the petrogenesis of Mariana trough magmas. *Earth and Planetary Science Letters*, *121*(3), 293-325.

Straub, S. M., Gómez-Tuena, A., Stuart, F. M., Zellmer, G. F., Espinasa-Perena, R., Cai, Y., Iizuka, Y. (2011). Formation of hybrid arc andesites beneath thick continental crust. *Earth and Planetary Science Letters*, *303*(3), 337-347.

Straub, S. M., LaGatta, A. B., Pozzo, M. D., Lillian, A., Langmuir, C. H. (2008) Evidence from high-Ni olivines for a hybridized peridotite/pyroxenite source for orogenic andesites from the central Mexican Volcanic Belt. *Geochemistry, Geophysics, Geosystems*, *9*(3).

Streck, M. J., Leeman, W. P., Chesley, J. (2007). High-magnesian andesite from Mount Shasta: A product of magma mixing and contamination, not a primitive mantle melt. *Geology*, *35*(4), 351-354.

Tatsumi, Y. (1981). Melting experiments on a high-magnesian andesite. *Earth and Planetary Science Letters*, *54*(2), 357-365.

Tatsumi, Y. (1982). Origin of high-magnesian andesites in the Setouchi volcanic belt, southwest Japan, II. Melting phase relations at high pressures. *Earth and Planetary Science Letters*, *60*(2), 305-317.

Tatsumi, Y. (2001). Geochemical modeling of partial melting of subducting sediments and subsequent melt-mantle interaction: Generation of high-Mg andesites in the Setouchi volcanic belt, southwest Japan. *Geology*, *29*(4), 323-326.

Tatsumi, Y. (2006). High-Mg andesites in the Setouchi volcanic belt, southwestern Japan: analogy to Archean magmatism and continental crust formation?. *Annu. Rev. Earth. Planet. Sci.*, *34*, 467-499.

Tatsumi, Y., Ishizaka, K. (1982). Origin of high-magnesian andesites in the Setouchi volcanic belt, southwest Japan, I. Petrographical and chemical characteristics. *Earth and Planetary Science Letters*, *60*(2), 293-304.

Till, C. B., Grove, T. L., Krawczynski, M. J. (2012a). A melting model for variably depleted and enriched lherzolite in the plagioclase and spinel stability fields. *Journal of Geophysical Research: Solid Earth (1978–2012)*, *117*(B6).

Till, C. B., Grove, T. L., Withers, A. C. (2012b). The beginnings of hydrous mantle wedge melting. *Contributions to Mineralogy and Petrology*, 1-20.

Tormey, D. R., Grove, T. L., Bryan, W. B. (1987). Experimental petrology of normal MORB near the Kane Fracture Zone: 22–25 N, mid-Atlantic ridge. *Contributions to Mineralogy and Petrology*, *96*(2), 121-139.

Walter, M. J. (1998). Melting of garnet peridotite and the origin of komatiite and depleted lithosphere. *Journal of Petrology*, *39*(1), 29-60.

Wasylenki, L. E., Baker, M. B., Kent, A. J., Stolper, E. M. (2003). Near-solidus melting of the shallow upper mantle: partial melting experiments on depleted peridotite. *Journal of Petrology*, *44*(7), 1163-1191.

Weaver, S. L., Wallace, P. J., Johnston, A. D. (2011). A comparative study of continental vs. intraoceanic arc mantle melting: Experimentally determined phase relations of hydrous primitive melts. *Earth and Planetary Science Letters*, *308*(1), 97-106.

Weber, J. N., Roy, R. (1965). Complex stable<--> metastable solid reactions illustrated with the Mg (OH) 2<--> MgO reaction. *American Journal of Science*, *263*(8), 668-677.

Weber, R. M., Wallace, P. J., Johnston, A. D. (2012). Experimental insights into the formation of high-Mg basaltic andesites in the trans-Mexican volcanic belt. *Contributions to Mineralogy and Petrology*, *163*(5), 825-840.

Watson, E., Wark, D., Price, J., Van Orman, J. (2002). Mapping the thermal structure of solid-media pressure assemblies. *Contributions to Mineralogy and Petrology*, *142*(6), 640-652.

Wood, B. J., Turner, S. P. (2009). Origin of primitive high-Mg andesite: Constraints from natural examples and experiments. *Earth and Planetary Science Letters*, *283*(1), 59-66.

Yoshii, T. (1974). The third Kurayoshi explosion and the crustal structure in the western part of Japan. *Journal of Physics of the Earth*, *22*, 109-121.

Zucca, J. J., Fuis, G. S., Milkereit, B., Mooney, W. D., Catchings, R. D. (1986). Crustal structure of northeastern California. *Journal of Geophysical Research: Solid Earth (1978–2012)*, *91*(B7), 7359-7382.

## *Figure Captions*

**Fig 1** **a)** Phase diagram with $H_2O$ content (wt%) from EPMA analyses v. Temperature (°C). Phase stability lines drawn for fertile mantle experiments at 1.2 GPa. Filled in quadrants indicate the presence of the corresponding phase. Pressures are indicated by color: 1.0 GPa is purple, 1.2 GPa is teal, 1.6 GPa is yellow, and 2.0 GPa is red. Squares are experiments conducted on fertile mantle compositions, and stars are experiments conducted on a depleted mantle composition.
**b)** Phase stability for fertile mantle melts. Pressure (GPa) v. melt fraction. The presence of a phase is indicated by symbol shape and color: experiments containing glass + ol are black squares, experiments with glass + ol + opx are dark grey diamonds, and experiments with glass + ol + opx + cpx are light grey circles.

**Fig 2** Comparison of $H_2O$ analyses from EPMA, ssr-FTIR, and SIMS. Black circles show $H_2O$ as measured by ssr-FTIR v. $H_2O$ measured by quantitative oxygen measurement on the EPMA. Grey circles show $H_2O$ measured by SIMS v. $H_2O$ measured by quantitative oxygen measurement on the EPMA.

**Fig 3** Back-scattered electron images of experiments C498 (top left), C508 (top right), and C554 (bottom). Images highlight the lack of quench crystals in melt pools. C498 and C508 were conducted in graphite+Pt capsules, and C554 was conducted in a Fe-saturated AuPd capsule. Vitreous carbon spheres are shown in C508. Run products for the experiments are labelled and listed in Table 2.

**Fig 4** Calculated v. experimental mineral components, temperature, pressure, and $H_2O$ for experimental glasses used to calibrate the model. Error bars correspond to the mean absolute error (mae, Table 6). Dashed lines indicate a ratio of 1:1 between the experimental and predicted values.

**Fig 5** Comparison of model calculations from this study (black circles) – T and P calculated using experimental $H_2O$ values; Lee et al. (2009, dark grey diamonds) – T (no P dependence) and P (with T Lee); and Wood and Turner (2009) (light grey triangles). Experiments used to calibrate the model were used in the model calculations for this study and the Lee et al. (2009), and only experiments presented in this paper with ol+opx±sp were calculated using the models of Wood and Turner (2009). In both pressure and temperature, our model is better at predicting the conditions of the experiments, as seen by the mean average error calculated for each model.

**Fig 6** Effect of pressure on primitive $H_2O$-undersaturated mantle melt compositions in pseudoternary projections as defined by Tormey et al (1987). Dashed arrows indicate the average movement of the four experimental glass compositions with increasing pressure. The grey arrows are model calculations for experiment C498. Mg # (molar ratio) = 0.78, $H_2O$ = 2.3 wt%, $Cr_2O_3$ = 0.29 wt%, NaK# (wt% ratio) = 0.20. Pressure was varied from 1.0-2.0 GPa to produce the grey vectors predicting the compositional change with pressure for this experiment.

**Fig 7** Effect of extent of melting in a pseudoternary projection through Cpx onto Ol-Plag-Qz (Tormey et al. 1987). Labels indicate the percentage of melt present in each experiment. Circles are 1.2 GPa experiments from this study with various amounts of $H_2O$; shaded region is a region defined by Baker and Stolper (1994)'s anhydrous 1.0 GPa experiments.

**Fig 8** Effect of water shown in a pseudoternary projection through Cpx onto Ol-Plag-Qz (Tormey et al. 1987). Labels indicate the percentage of $H_2O$ in the glass of experiments at 1.2 GPa. Circles are experiments from this study with variable amounts of $H_2O$; color indicates pressure (Purple = 1.0 GPa; Teal = 1.2 GPa; Yellow = 1.6 GPa; Red = 2.0 GPa). The shaded teal region is the anhydrous origin defined by experiments from this study (labelled Anhydrous). The purple region to the right is defined by Baker and Stolper (1994)'s anhydrous 1.0 GPa experiments. Purple plus signs are 1.0 GPa $H_2O$ – undersaturated experiments by Hirose and Kawamoto (1995), and purple diamonds are 1.0 GPa $H_2O$-saturated runs by Hirose (1997).

**Fig 9** Element (wt%) v. MgO (wt%). This figure compares the compositions of our experiments with natural PAs and inclusions from Mt. Shasta, CA. The distinct regions defined by the locations of the samples are particularly notable in $SiO_2$, CaO, $Na_2O$, and FeO. Primitive experiments from this study are circles. Black circle = 2.0 GPa, Dark grey circle = 1.6 GPa, Light grey circle = 1.2 GPa, and White circle = 1.0 GPa. Depleted experiments (1.2 GPa) are stars. Natural samples are diamonds; pink – Setouchi (Tatsumi and Ishizaka 1982); Orange – Kamchatka (Bryant et al. 2010); Cyan – Cascades (Grove et al 2002; Barr 2010); Black – Trans-Mexico Volcanic Belt (Weaver et al. 2011; Weber et al. 2011, Meriggi et al. 2008). The shaded region is the inclusions from Mt. Shasta (Krawczynski and Grove, in prep). In CaO v. MgO, the arrow indicates change in glass composition with higher extents of melting, dotted lines indicate melting paths for the depleted composition, and the blue square is the glass composition of D206, a 3.2 GPa $H_2O$-saturated experiment from Till et al. (2012).

**Fig 10** Model results plotted on pseudoternary diagrams as defined by Tormey et al. (1987) for melts in equilibrium with olivine and orthopyroxene using fixed values for $Cr_2O_3$ (0.28) and NaK# (0.19). Results are shown at 0.8, 1.0, 1.5, and 2.0 GPa with $H_2O$ varying from 0-9 wt% (left→right), and Mg# varying from 0.71-0.86 (top→bottom; bounds chosen by the limits of the model calibration). 0.8 GPa is dashed because the model is only calibrated between 1.0-2.5 GPa. Natural PA lava data (Table 7) is superimposed on the model results. Symbols are same as in Figure 9. Arrows ($H_2O$ vectors shown in the 0.8 GPa result) show the effect of $H_2O$ on melt composition at a given pressure and melt extent.
**a)** Pseudoternary projection through Plag onto Ol-Cpx-Qz (Tormey et al. 1987).
**b)** Pseudoternary projection through Cpx onto Ol-Plag-Qz (Tormey et al. 1987).

**Fig 12** Predicted $H_2O$ v. measured $SiO_2$ of natural PAs from Kamchatka, Setouchi, Cascades, and Mexico. Symbols the same as in Figure 9.

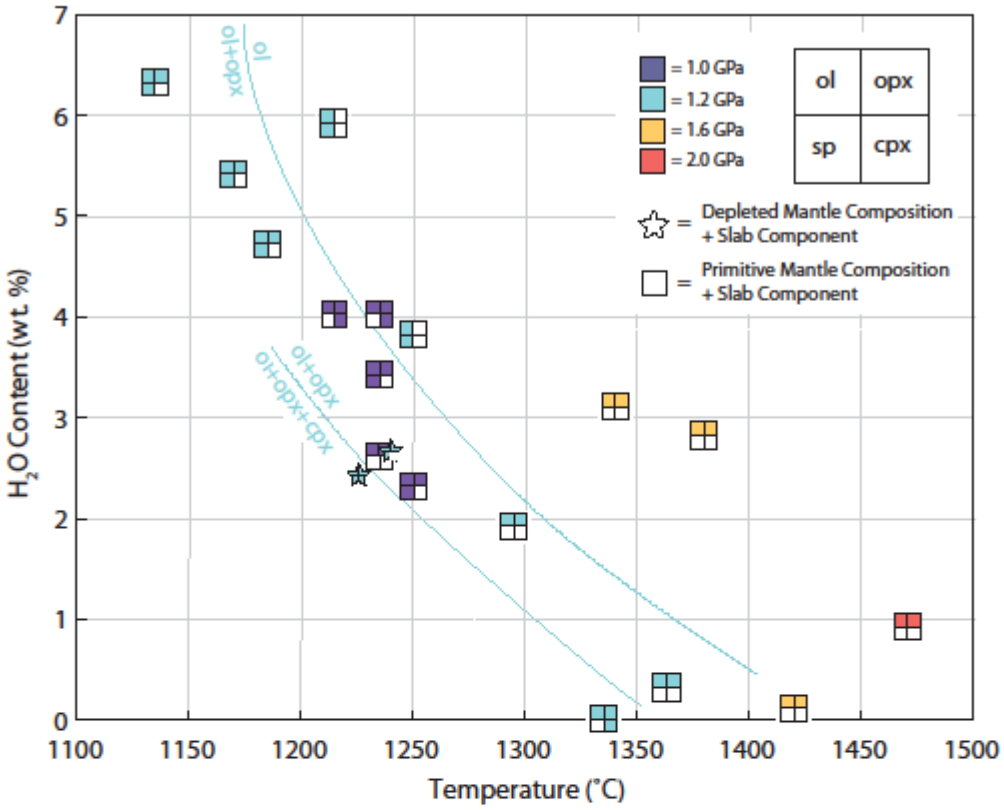
7
6
5
4
3
2
1
0
1100
1150
1200
1250
1300
1350
1400
1450
1500
H2O Content (wt.%)
Temperature (°C)
ol
ol+opx
ol+opx
ol+opx+cpx
= 1.0 GPa
= 1.2 GPa
= 1.6 GPa
= 2.0 GPa
ol
opx
sp
cpx
= Depleted Mantle Composition + Slab Component
= Primitive Mantle Composition + Slab Component

**Figure 1a**

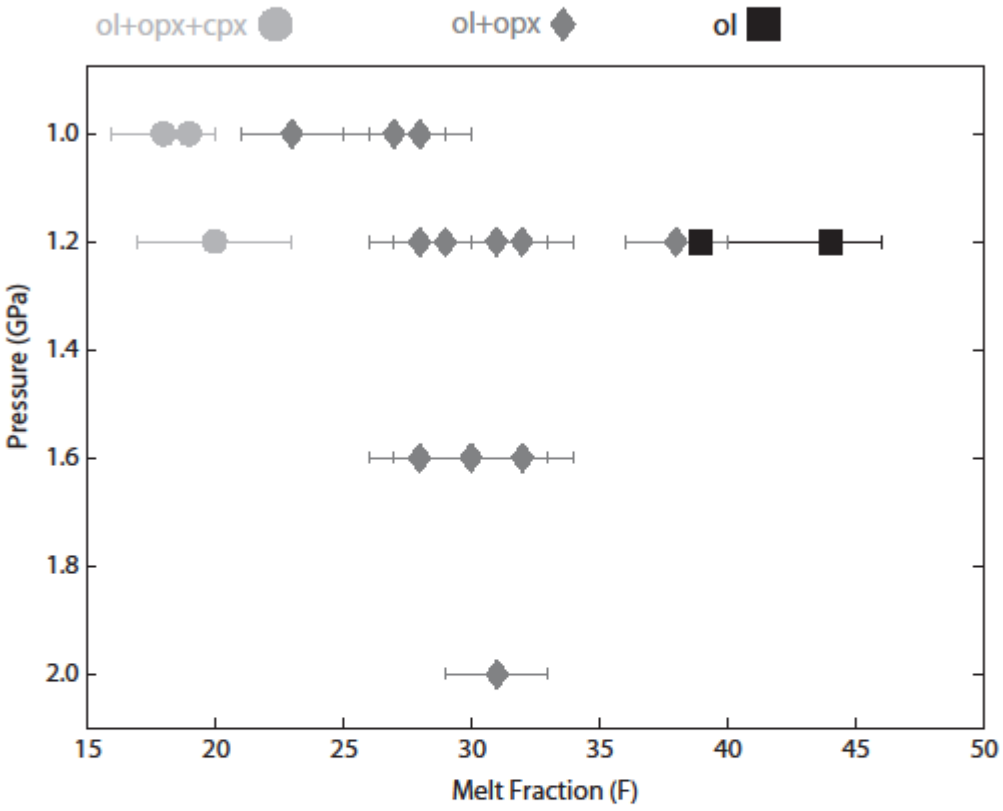
ol+opx+cpx
ol+opx
ol
Pressure (GPa)
1.0
1.2
1.4
1.6
1.8
2.0
15
20
25
30
35
40
45
50
Melt Fraction (F)

**Figure 1b**

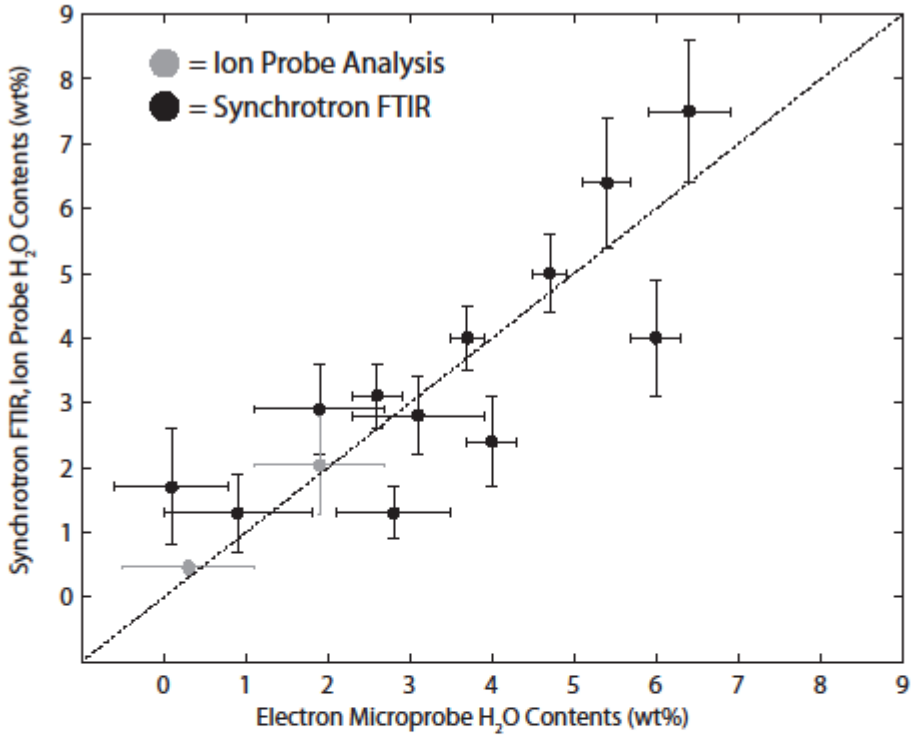
= Ion Probe Analysis
= Synchrotron FTIR
Synchrotron FTIR, Ion Probe $H_2O$ Contents (wt%)
Electron Microprobe $H_2O$ Contents (wt%)
0
1
2
3
4
5
6
7
8
9

**Figure 2**

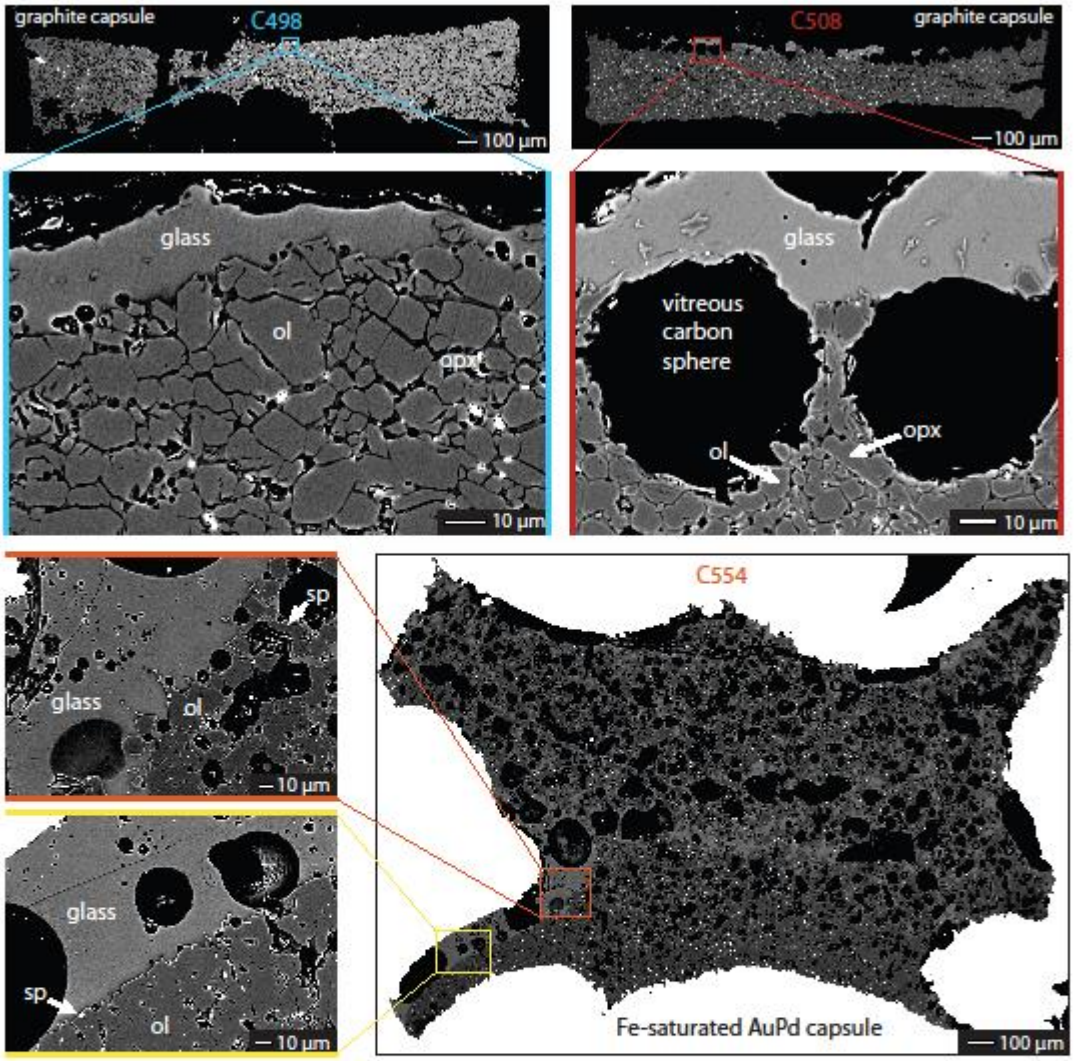
graphite capsule
C498
100 µm
C508
graphite capsule
100 µm
glass
ol
opx
10 µm
glass
vitreous
carbon
sphere
opx
ol
10 µm
sp
glass
ol
10 µm
C554
glass
sp
ol
10 µm
Fe-saturated AuPd capsule
100 µm

**Figure 3**

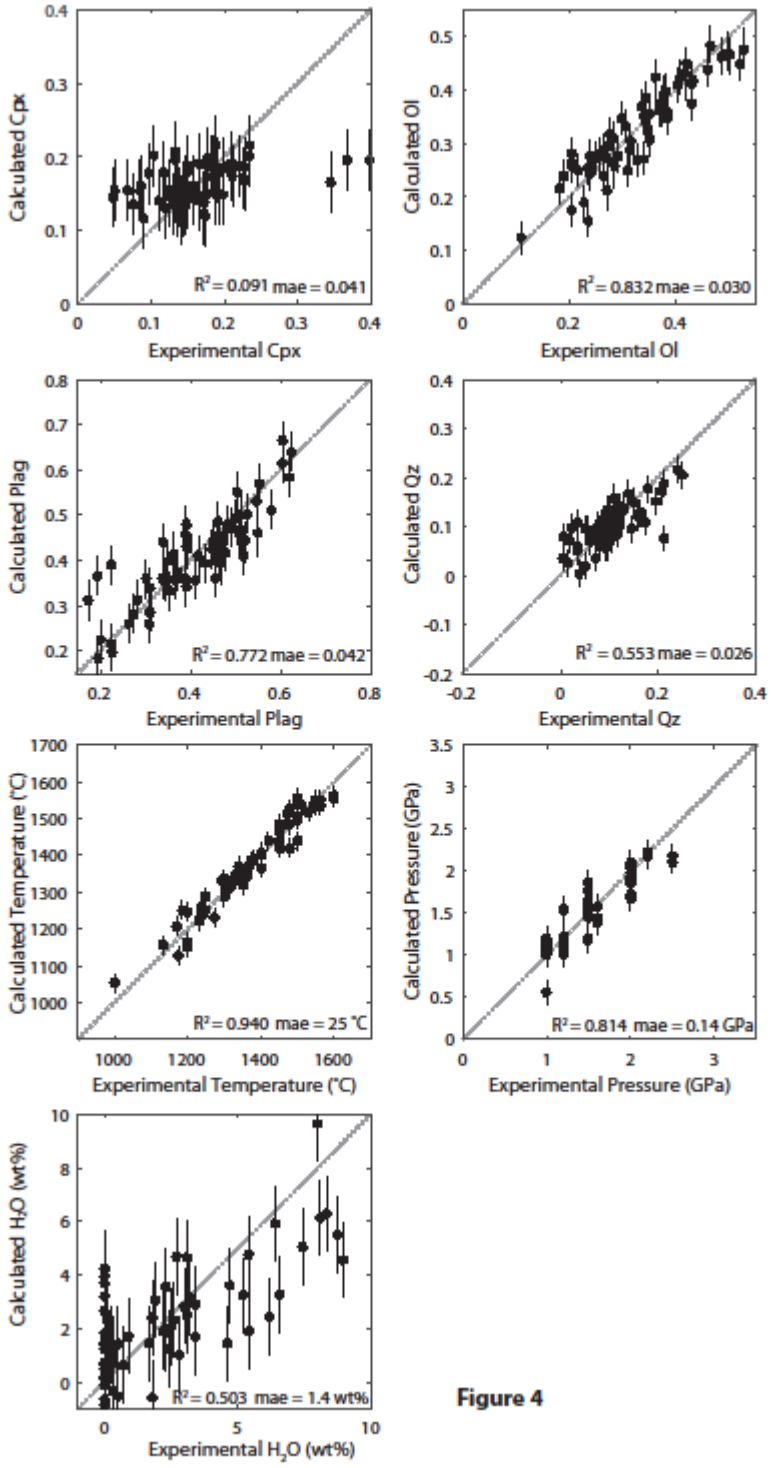
Calculated Cpx
Experimental Cpx
R² = 0.091 mae = 0.041
Calculated Ol
Experimental Ol
R² = 0.832 mae = 0.030
Calculated Plag
Experimental Plag
R² = 0.772 mae = 0.042
Calculated Qz
Experimental Qz
R² = 0.553 mae = 0.026
Calculated Temperature (°C)
Experimental Temperature (°C)
R² = 0.940 mae = 25 °C
Calculated Pressure (GPa)
Experimental Pressure (GPa)
R² = 0.814 mae = 0.14 GPa
Calculated H2O (wt%)
Experimental H2O (wt%)
R² = 0.503 mae = 1.4 wt%

**Figure 4**

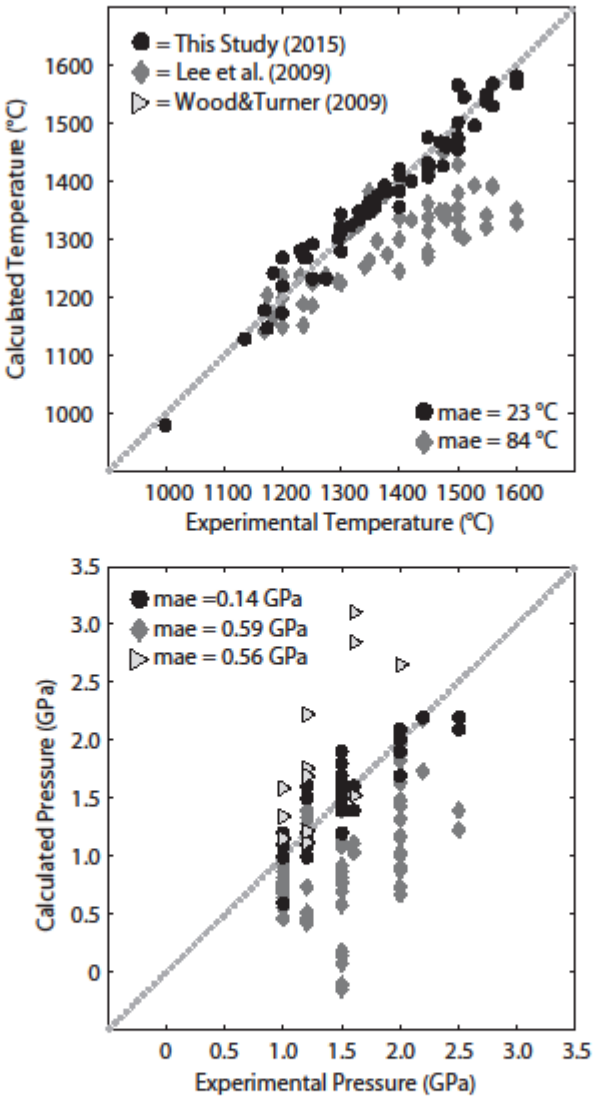
= This Study (2015)
= Lee et al. (2009)
= Wood&Turner (2009)
mae = 23 °C
mae = 84 °C
Calculated Temperature (°C)
Experimental Temperature (°C)
1000
1100
1200
1300
1400
1500
1600
mae =0.14 GPa
mae = 0.59 GPa
mae = 0.56 GPa
Calculated Pressure (GPa)
Experimental Pressure (GPa)
0
0.5
1.0
1.5
2.0
2.5
3.0
3.5

**Figure 5**

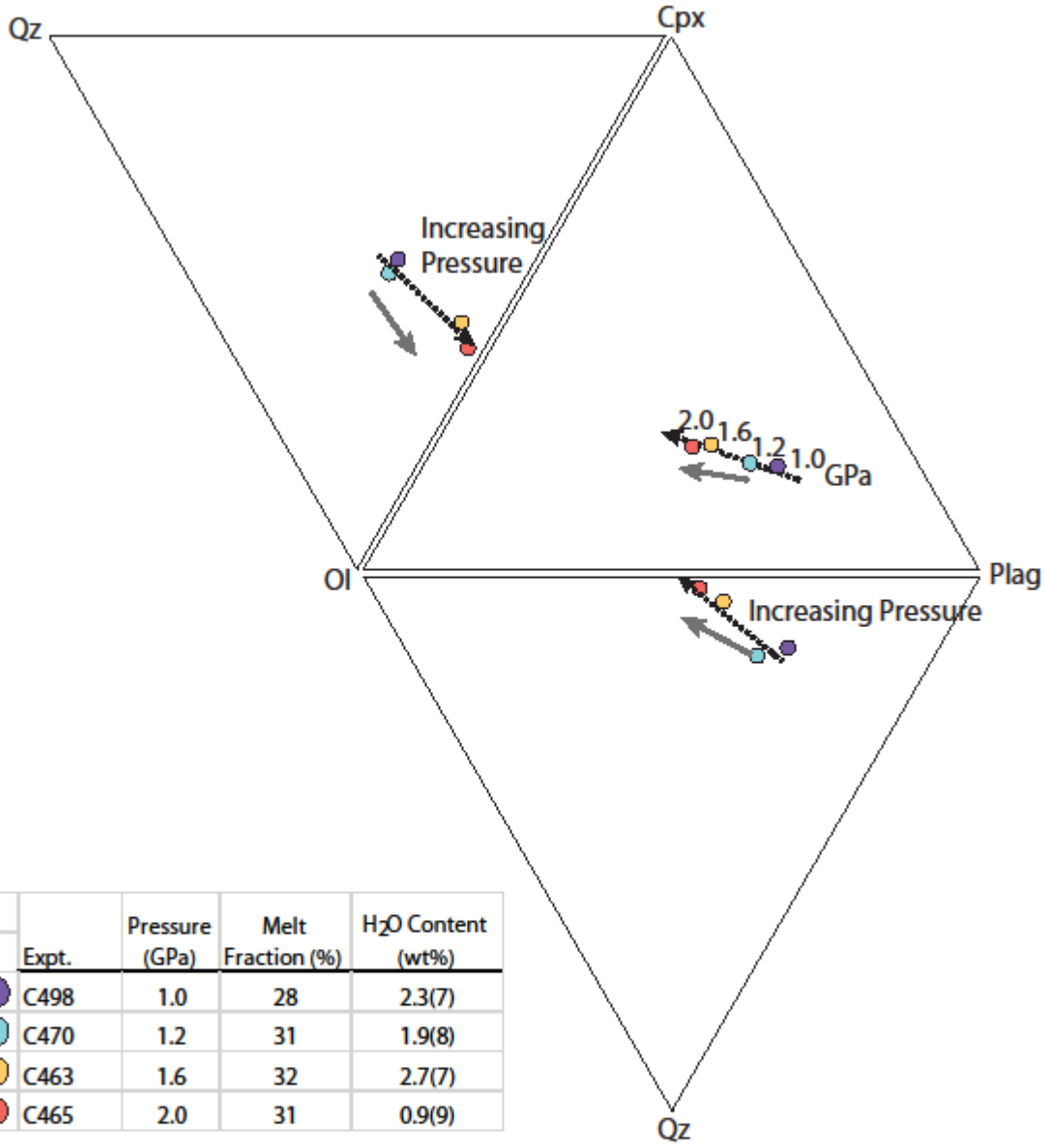


| | Expt. | Pressure (GPa) | Melt Fraction (%) | $H_2O$ Content (wt%) |
|---|---|---|---|---|
| ● | C498 | 1.0 | 28 | 2.3(7) |
| ● | C470 | 1.2 | 31 | 1.9(8) |
| ● | C463 | 1.6 | 32 | 2.7(7) |
| ● | C465 | 2.0 | 31 | 0.9(9) |

**Figure 6**

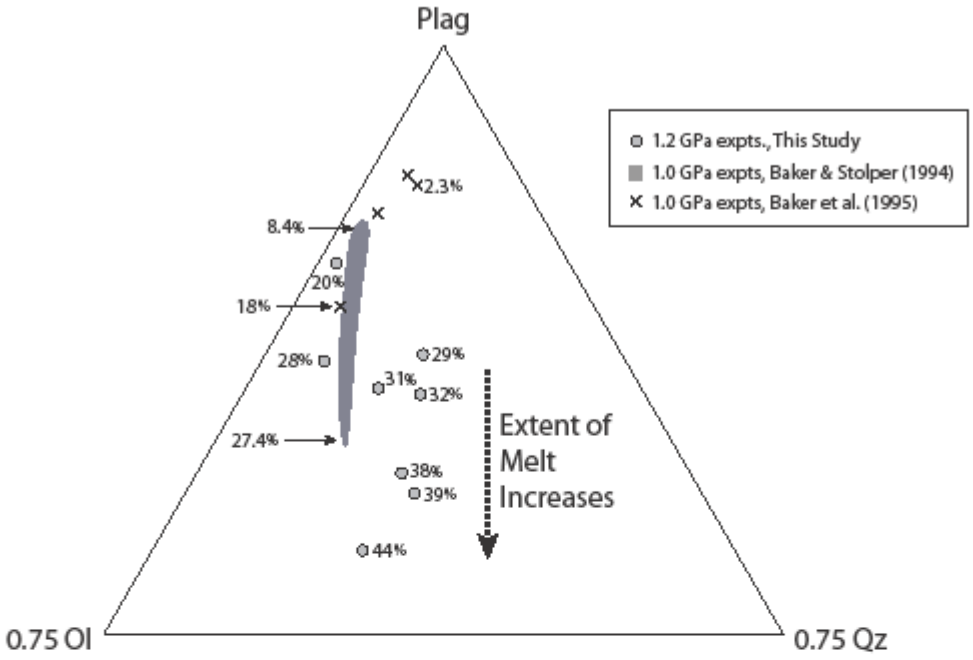
Plag
1.2 GPa expts., This Study
1.0 GPa expts, Baker & Stolper (1994)
1.0 GPa expts, Baker et al. (1995)
2.3%
8.4%
20%
18%
28%
29%
31%
32%
27.4%
38%
39%
44%
Extent of Melt Increases
0.75 Ol
0.75 Qz

**Figure 7**

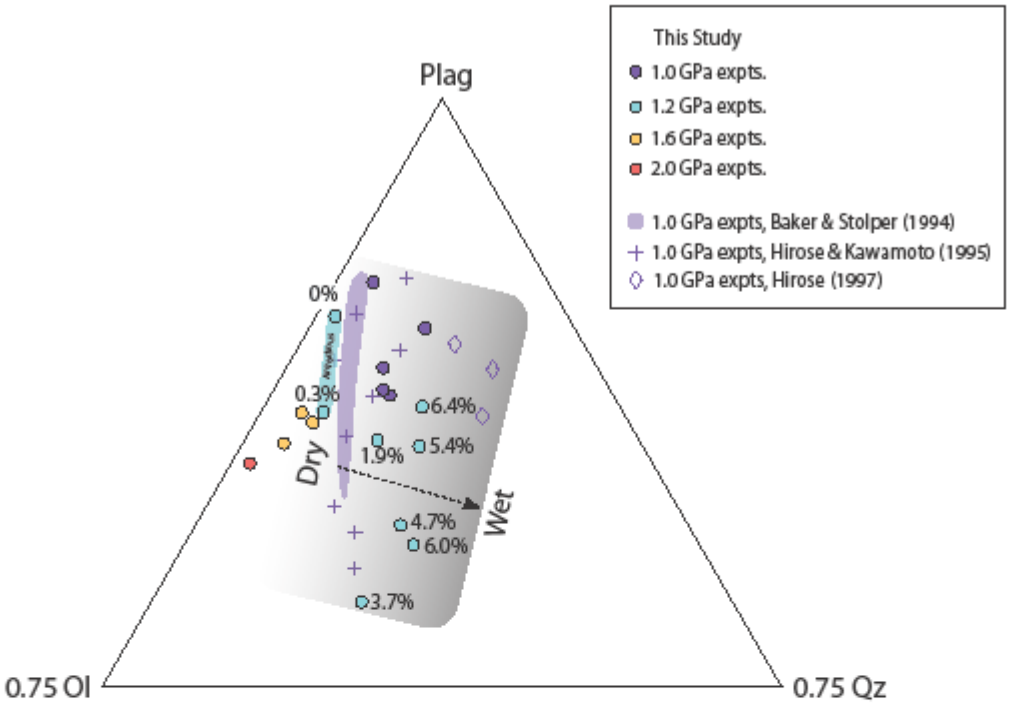
This Study
1.0 GPa expts.
1.2 GPa expts.
1.6 GPa expts.
2.0 GPa expts.
1.0 GPa expts, Baker & Stolper (1994)
1.0 GPa expts, Hirose & Kawamoto (1995)
1.0 GPa expts, Hirose (1997)
Plag
0.75 Ol
0.75 Qz
0%
0.3%
1.9%
5.4%
6.4%
4.7%
6.0%
3.7%
Dry
Wet

**Figure 8**

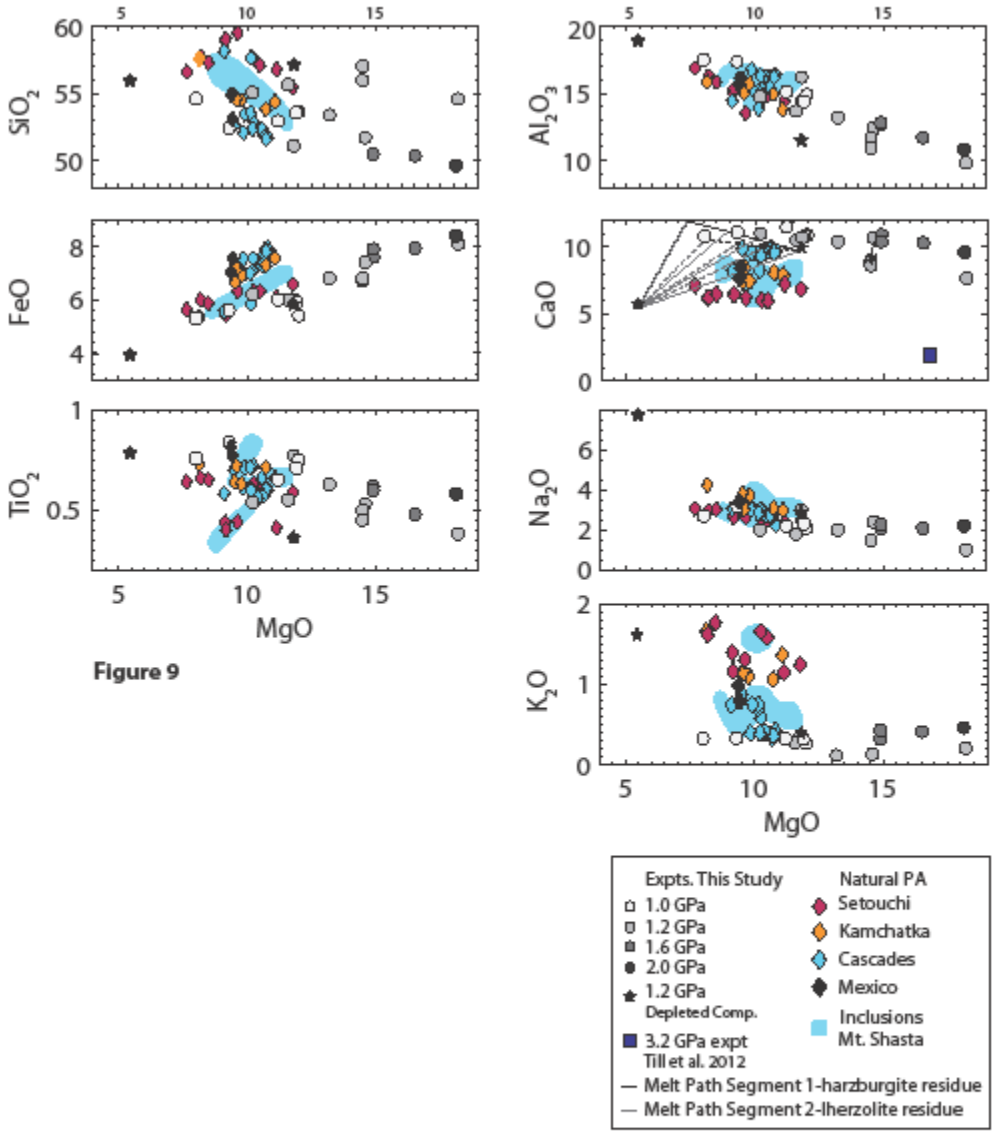
SiO2
FeO
TiO2
MgO
Al2O3
CaO
Na2O
K2O
MgO
Expts. This Study
1.0 GPa
1.2 GPa
1.6 GPa
2.0 GPa
1.2 GPa
Depleted Comp.
3.2 GPa expt
Till et al. 2012
Natural PA
Setouchi
Kamchatka
Cascades
Mexico
Inclusions
Mt. Shasta
Melt Path Segment 1-harzburgite residue
Melt Path Segment 2-lherzolite residue

**Figure 9**

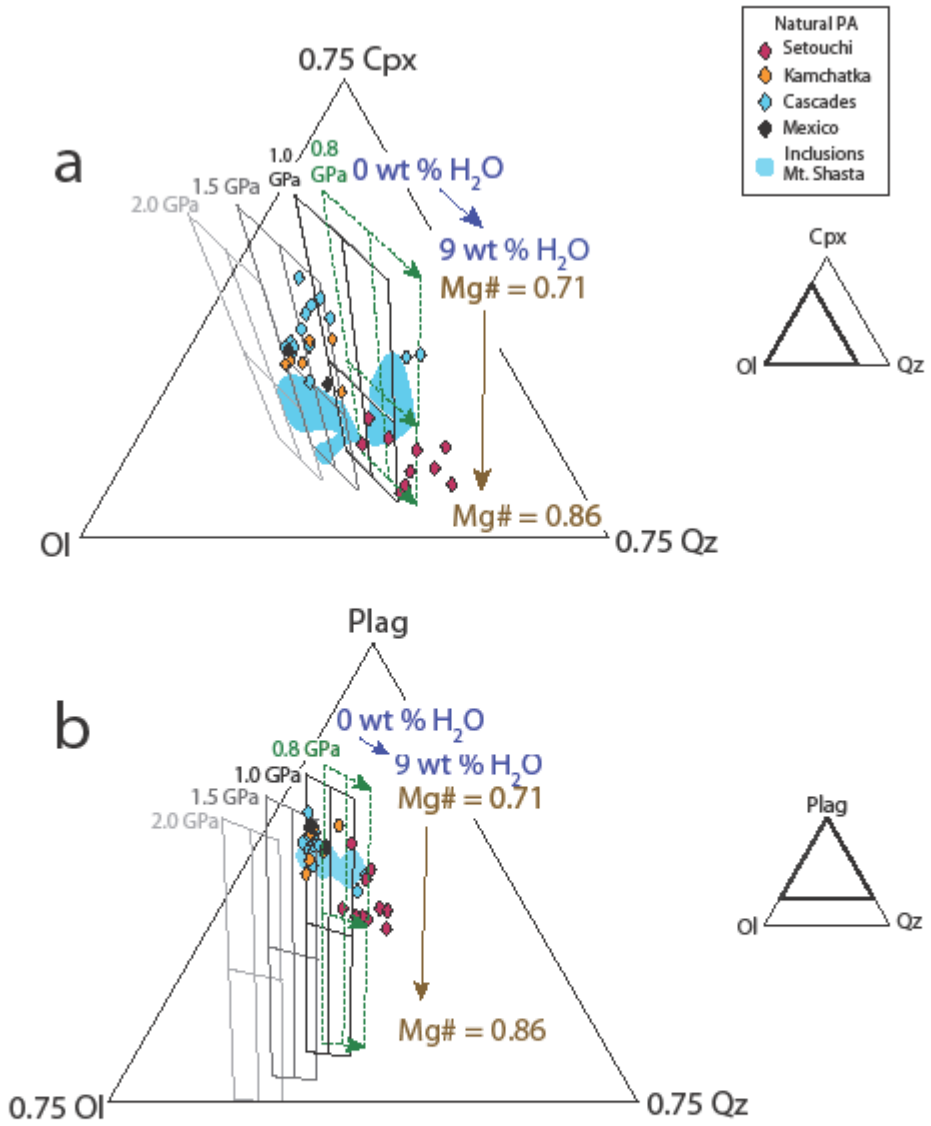
a
0.75 Cpx
0.8 GPa
1.0 GPa
1.5 GPa
2.0 GPa
0 wt % H2O
9 wt % H2O
Mg# = 0.71
Mg# = 0.86
Ol
0.75 Qz
Natural PA
Setouchi
Kamchatka
Cascades
Mexico
Inclusions Mt. Shasta
Cpx
Ol
Qz
b
Plag
0 wt % H2O
9 wt % H2O
0.8 GPa
1.0 GPa
1.5 GPa
2.0 GPa
Mg# = 0.71
Mg# = 0.86
0.75 Ol
0.75 Qz
Plag
Ol
Qz

**Figure 10**

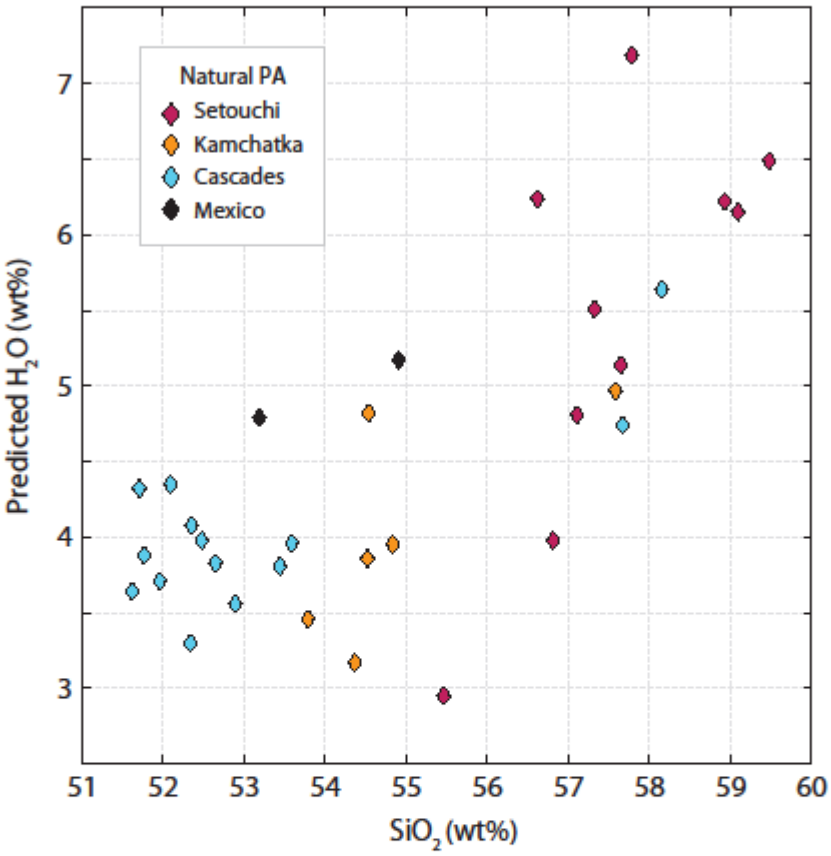
Natural PA
Setouchi
Kamchatka
Cascades
Mexico
Predicted $H_2O$ (wt%)
$SiO_2$ (wt%)
3
4
5
6
7
51
52
53
54
55
56
57
58
59
60

**Figure 11**

**Table 1** Composition of Starting Materials *(wt %)*

| Mix | ω H&Z + $H_2O$[b] | A H&Z Dry + SM[c] | B[a] 11% H&Z + $H_2O$ | C[a] 22% H&Z + $H_2O$ | D[a] 29% H&Z + $H_2O$ | E[a] 41% H&Z + $H_2O$ | F Dry Depleted Composition[c] |
|---|---|---|---|---|---|---|---|
| $SiO_2$ | 46.20 | 46.34 | 46.32 | 46.31 | 46.30 | 46.28 | 44.06 |
| $TiO_2$ | 0.18 | 0.18 | 0.18 | 0.18 | 0.18 | 0.18 | 0.08 |
| $Al_2O_3$ | 4.06 | 4.27 | 4.25 | 4.22 | 4.21 | 4.18 | 2.17 |
| $Cr_2O_3$ | 0.40 | 0.40 | 0.40 | 0.40 | 0.40 | 0.40 | 0.45 |
| FeO | 7.56 | 7.45 | 7.46 | 7.47 | 7.48 | 7.49 | 8.04 |
| MnO | 0.10 | 0.10 | 0.10 | 0.10 | 0.10 | 0.10 | 0.12 |
| MgO | 37.82 | 36.92 | 37.02 | 37.12 | 37.18 | 37.29 | 42.10 |
| CaO | 3.22 | 3.19 | 3.19 | 3.19 | 3.20 | 3.20 | 1.99 |
| $Na_2O$ | 0.33 | 0.69 | 0.65 | 0.61 | 0.59 | 0.54 | 0.59 |
| $K_2O$ | 0.03 | 0.20 | 0.18 | 0.16 | 0.15 | 0.13 | 0.13 |
| NiO | 0.28 | 0.28 | 0.28 | 0.28 | 0.28 | 0.28 | 0.28 |
| Sum | 100.18 | 100.00 | 100.02 | 100.04 | 100.05 | 100.08 | 100.01 |
| $H_2O$ | 14.50 | 0.00 | 1.60 | 3.19 | 4.21 | 5.95 | 0.00 |
| Mg# | 0.90 | 0.90 | 0.90 | 0.90 | 0.90 | 0.90 | 0.90 |

[a]*Mixes B-E are displayed as percent of the H&Z + H2O mix (ω). The remainder of the composition is Mix A. For example, Mix B=11% Mix ω + 89% Mix A.*

[b]Till et al. (2012b)

[c]Slab Melt added as an additional alkali component

**Table 2** Experimental run conditions, phase proportions and uncertainties, and $K_D$s

| Expt. | P (GPa) | T (°C) | Time (hrs) | Mix[a] | Phase Proportions (Uncertainties[b]) Gl | Ol | Opx | Cpx | Sp | $H_2O$ Concentrations (Uncertainties[b]) EMPA | Synch. | Ion Probe | $K_D$ Ol | Opx | Cpx | Fe Gain/ Loss | Capsule[c] | Traps[d] |
|---|---|---|---|---|---|---|---|---|---|---|---|---|---|---|---|---|---|---|
| Primitive Mantle Composition | | | | | | | | | | | | | | | | | | |
| C507 | 1.0 | 1215 | 31 | E | 19(1) | 53(3) | 23(4) | 5(1) | | 3.8(3) | | | 0.29 | 0.24 | 0.26 | 0.0 | g | |
| C508 | 1.0 | 1235 | 8 | E | 23(2) | 48(8) | 29(10) | | | 2.6(3) | 3.1(5) | | 0.34 | 0.32 | | -7.1 | g | CS |
| C494 | 1.0 | 1235 | 49 | D | 18(2) | 50(5) | 25(7) | 7(4) | | 4.0(3) | 2.4(3) | | 0.30 | 0.28 | 0.26 | -4.3 | g | |
| C490 | 1.0 | 1235 | 72 | D | 27(2) | 69(5) | 4(6) | | 0.4(0.1) | 3.4(6) | | | 0.33 | 0.34 | | -8.9 | g | |
| C498 | 1.0 | 1250 | 46 | B | 28(2) | 68(5) | 4(7) | | 0.3(0.1) | 2.2(7) | | | 0.31 | 0.32 | | -12 | g | |
| C561 | 1.2 | 1135 | 27 | E | 29(2) | 64(5) | 7(7) | | tr[e] | 6.4(5) | 7.5(1.1) | | 0.31 | 0.29 | | 8.3 | Au-Pd | |
| C555 | 1.2 | 1170 | 24 | E | 32(2) | 61(5) | 7(7) | | tr[e] | 5.4(3) | 6.4(1.0) | | 0.33 | 0.32 | | 0.3 | Au-Pd | |
| C554 | 1.2 | 1185 | 24 | E | 38(2) | 56(5) | 6(7) | | tr[e] | 4.7(2) | 5.0(6) | | 0.34 | 0.33 | | 0.9 | Au-Pd | |
| C553 | 1.2 | 1215 | 24 | E | 39(3) | 61(3) | | | 0.5(0) | 6.0(3) | 4.0(9) | | 0.32 | | | 0 | Au-Pd | |
| C559 | 1.2 | 1250 | 25 | E | 44(2) | 55(2) | | | 0.5(0) | 3.7(2) | 4.0(5) | | 0.34 | | | 6.1 | Au-Pd | |
| C470 | 1.2 | 1295 | 72 | C | 31(2) | 59(5) | 10(7) | | | 1.9(8) | 2.9(7) | 2.04(0.752) | 0.30 | 0.30 | | -3.4 | g | CS |
| C481 | 1.2 | 1335 | 72 | A | 20(3) | 50(7) | 17(8) | 14(11) | | 0(1) | | | 0.36 | 0.35 | 0.37 | 0.3 | g | CS |
| C471 | 1.2 | 1363 | 61 | A | 28(2) | 54(5) | 18(7) | | | 0.3(8) | | 0.460(0.108) | 0.34 | 0.33 | | 3.1 | g | CS |
| C473 | 1.6 | 1340 | 73 | C | 30(3) | 53(5) | 17(6) | | | 3.1(8) | 2.8(6) | | 0.31 | 0.30 | | -1.5 | g | |
| C463 | 1.6 | 1380 | 73 | B | 32(2) | 54(5) | 14(6) | | | 2.8(7) | 1.3(4) | | 0.32 | 0.31 | | -4.0 | g | |
| C474 | 1.6 | 1420 | 72 | A | 28(2) | 52(4) | 20(6) | | | 0.1(7) | 1.7(9) | | 0.32 | 0.31 | | 2.2 | g | |
| C465 | 2.0 | 1470 | 72 | A | 31(2) | 49(4) | 20(5) | | | 0.9(9) | 1.3(6) | | 0.32 | 0.31 | | 1.2 | g | |

**Table 3** Calculated $fO_2$ of Fe saturated AuPd experiments, Barr and Grove (2010) Model 1

| | All Fe as FeO | | $Fe^{3+}$ correction using Kress & Carmichael (1991), 5 iterations | |
|---|---|---|---|---|
| Expt. | $\log_{10} fO_2$ | QFM + | $\log_{10} fO_2$ | QFM + |
| C561 | -10.502 (0.175) | -2.4 | -10.600 (0.175) | -2.4 |
| C555 | -9.479 (0.039) | -1.7 | -9.604 (0.039) | -1.9 |
| C554 | -9.010 (0.086) | -1.4 | -9.146 (0.086) | -1.6 |
| C553 | -8.646 (0.082) | -1.4 | -8.780 (0.082) | -1.5 |
| C559 | -8.297 (0.049) | -1.4 | -8.424 (0.049) | -1.5 |

**Table 4** Electron microprobe analyses of experimental run products (*wt%*)

| Expt. | Phase | n[a] | $SiO_2$ | $TiO_2$ | $Al_2O_3$ | $Cr_2O_3$ | FeO[b] | MnO | MgO | CaO | $Na_2O$ | $Na_2O_{CORR}$[c] | $K_2O$ | $P_2O_5$ | NiO | $H_2O$ | Sum |
|---|---|---|---|---|---|---|---|---|---|---|---|---|---|---|---|---|---|
| Primitive Mantle Composition | | | | | | | | | | | | | | | | | |
| *1.0 GPa Experiments* | | | | | | | | | | | | | | | | | |
| C507 | gl | 2 | 53.2(1) | 0.73(1) | 17.0(1) | 0.13(1) | 5.1(1) | 0.14(4) | 7.84(8) | 10.28(3) | 2.0(2) | 2.7 | 0.32(2) | 0.01(1) | | 3.8(3) | 100.6(4) |
| | ol | 7 | 40.7(3) | 0.01(1) | 0.1(2) | 0.11(2) | 9.3(2) | 0.12(2) | 49.7(5) | 0.21(8) | | | | | 0.26(5) | | 100.5(4) |
| | opx | 2 | 56.1(5) | 0.08(1) | 2.6(4) | 1.00(6) | 5.0(3) | 0.11(2) | 32.1(3) | 1.97(1) | 0.04(2) | | | | | | 99.06(4) |
| | cpx | 4 | 53.3(6) | 0.18(2) | 3.4(4) | 1.5(2) | 3.4(2) | 0.10(4) | 20(1) | 18(1) | 0.30(6) | | | | | | 100.4(3) |
| C508 | gl | 22 | 52.1(4) | 0.65(8) | 14.9(4) | 0.21(4) | 5.9(3) | 0.14(2) | 11.1(8) | 11.0(3) | 1.8(2) | 2.2 | 0.32(3) | 0.02(2) | | 2.6(3) | 100.8(4) |
| | ol | 7 | 40.8(5) | | 0.05(7) | 0.18(2) | 8.9(2) | 0.10(2) | 50.0(5) | 0.22(4) | | | | | 0.35(3) | | 100.6(5) |
| | opx | 6 | 55.5(7) | 0.12(2) | 2.0(3) | 0.9(1) | 5.6(1) | 0.12(3) | 33(1) | 2.2(5) | 0.03(2) | | | | | | 99.8(2) |
| C494 | gl | 8 | 51.2(2) | 0.8(1) | 17.0(4) | 0.08(6) | 5.5(1) | 0.07(2) | 9.0(5) | 10.5(2) | 2.1(1) | 3.2 | 0.32(1) | 0.01(2) | | 4.0(3) | 100.5(2) |
| | ol | 6 | 40.8(1) | 0.02(2) | 0.06(4) | 0.11(5) | 9.1(2) | 0.13(1) | 49.4(3) | 0.19(1) | | | | | 0.12(3) | | 100.0(3) |
| | opx | 6 | 56.5(4) | 0.13(3) | 2.5(6) | 0.94(9) | 5.5(2) | 0.10(3) | 32.7(5) | 2.1(1) | 0.04(4) | | | | | | 100.6(3) |
| | cpx | 3 | 53.6(3) | 0.20(2) | 3.1(6) | 1.4(2) | 3.1(2) | 0.07(2) | 20.3(6) | 19.2(8) | 0.32(2) | | | | | | 101.3(2) |
| C490 | gl | 15 | 52.2(4) | 0.7(1) | 14.5(2) | 0.23(3) | 5.2(3) | 0.10(2) | 11.7(5) | 10.3(3) | 1.9(2) | 2.1 | 0.25(2) | | | 3.4(6) | 100.6(7) |
| | ol | 5 | 40.79(2) | | 0.04(2) | 0.15(1) | 7.6(3) | 0.12(4) | 51.1(1) | 0.21(2) | | | | | 0.06(3) | | 100.1(4) |
| | opx | 4 | 56.3(3) | 0.07(1) | 2.1(2) | 1.07(4) | 5.1(3) | 0.06(3) | 33.5(2) | 1.79(9) | 0.04(3) | | | | | | 100.0(5) |
| | sp | 5 | 0.2(1) | 0.27(4) | 20(1) | 51.3(5) | 11.8(3) | 0.17(6) | 16.6(6) | 0.07(1) | | | | | 0.02(3) | | 100.0(9) |
| C498 | gl | 10 | 52.8(6) | 0.7(1) | 14.2(5) | 0.29(6) | 5.8(2) | 0.12(3) | 12(1) | 10.4(3) | 1.7(2) | 2.3 | 0.30(3) | 0.03(1) | | 2.2(7) | 100.3(6) |
| | ol | 8 | 41.1(5) | | 0.03(1) | 0.19(2) | 8.0(2) | 0.04(2) | 50.8(4) | 0.2(1) | | | | | 0.09(3) | | 100.5(9) |
| | opx | 5 | 57.1(4) | 0.07(2) | 1.7(2) | 1.0(0) | 5.4(3) | 0.10(1) | 33.6(4) | 1.58(6) | 0.05(1) | | | | | | 100.6(8) |
| | sp | 4 | 0.2(1) | 0.30(3) | 19.4(4) | 50.6(2) | 11.5(3) | 0.20(9) | 16.9(1) | 0.15(7) | | | | | 0.04(2) | | 99.3(3) |
| *1.2 GPa Experiments* | | | | | | | | | | | | | | | | | |
| C561 | gl | 6 | 51.9(8) | 0.50(3) | 14.0(1) | 0.10(1) | 5.8(1) | 0.11(1) | 9.6(4) | 10.0(3) | 1.5(2) | 2.0 | 0.29(1) | | 0.01(1) | 6.4(5) | 100.1(3) |
| | ol | 8 | 40.6(2) | | 0.01(1) | | 9.3(2) | 0.09(1) | 49.9(2) | 0.07(1) | | | | | 0.30(5) | | 100.3(3) |
| | opx | 8 | 56.6(2) | 0.08(1) | 1.3(2) | 0.71(9) | 6.0(1) | 0.11(1) | 33.5(2) | 1.34(8) | 0.03(3) | | 0.004(4) | | | | 99.7(2) |

**Table 5** Experimental Data Used in Model

| Reference | # of Glasses Used | Experiments |
|---|---|---|
| This Study | 12 | C463, C465, C470, C471, C473, C474, C490, C498, C508, C554, C555, C561 |
| Falloon and Danyushevsky (2000) | 23 | T-3569, T-3572, T-4347, T-4348, T-4350, T-4349, T-4351, T-4316, T-4312, T-3486, T-3471, T-3520, T-3521, T-3538, T-3564, T-3565, T-3490, T-3494, T-3385, T-3387, T-3488, T-3516, T-3514 |
| Gaetani and Grove (1998) | 3 | B305, B384, B388 |
| Hirose (1997) | 1 | 49 |
| Hirose and Kawamoto (1995) | 4 | 39, 42, 43, 44 |
| Laporte et al. (2004) | 3 | 8, 17, 6 |
| | 7 | rev2g, rev6a, rev6b, rev8a, rev8b, rec8c, rev8d |
| Parman and Grove (2004) | 12 | BK2.19, BK2.20, BK2.28, W.9, W.11, W.20, W.22, W3.31, W3.32, W3.33, W3.35, W3.36 |
| **Total** | **65** | |

*Removed for silica undersaturation

**Table 6** Model Equations Produced by Multiple Linear Regression of Experimental Liquids[a]

| | | | | | | | | | | | | | | | | | | | | | AIC[b] | $r^2$ | Mean Abs. Error[c] |
|---|---|---|---|---|---|---|---|---|---|---|---|---|---|---|---|---|---|---|---|---|---|---|---|
| P | = | -2.53 | + | 0.0535 | ($H_2O$) | + | 0.429 | ($TiO_2$) | - | 0.453 | ($Cr_2O_3$) | + | 3.55 | (Cpx) | + | 6.81 | (Ol) | + | 2.40 | (Plag) | -25.7 | 0.814 | 0.14 GPa |
| | | *0.54* | | *0.0102* | | | *0.111* | | | *0.146* | | | *0.57* | | | *0.66* | | | *0.57* | | | | |
| $H_2O$ | = | -16.3 | + | 5.28 | (P) | + | 36.1 | (1-Mg#) | + | 8.79 | (Plag) | - | 12.0 | (Ol) | + | 30.6 | (Qz) | | | | 273.79 | 0.503 | 1.4 wt% |
| | | *4.8* | | *0.90* | | | *14.2* | | | *4.06* | | | *6.5* | | | *6.4* | | | | | | | |
| T | = | 1326 | + | 171 | (P) | - | 826 | (1-Mg#) | - | 27.6 | ($H_2O$) | + | 102 | ($Cr_2O_3$) | | | | | | | 640.29 | 0.940 | 25°C |
| | | *53* | | *11* | | | *177* | | | *1.8* | | | *23* | | | | | | | | | | |
| Cpx | = | -0.0482 | + | 0.0307 | (P) | + | 0.771 | (1-Mg#) | - | 0.0752 | (NaK#) | - | 0.00660 | ($H_2O$) | + | 0.0906 | ($Cr_2O_3$) | | | | -174.2 | 0.091 | 0.041 |
| | | *0.1139* | | *0.0216* | | | *0.364* | | | *0.1253* | | | *0.00350* | | | *0.0482* | | | | | | | |
| Oliv | = | 0.521 | + | 0.111 | (P) | - | 1.51 | (1-Mg#) | - | 0.199 | (NaK#) | - | 0.00320 | ($H_2O$) | + | 0.00280 | ($Cr_2O_3$) | | | | -236.5 | 0.832 | 0.030 |
| | | *0.071* | | *0.013* | | | *0.23* | | | *0.078* | | | *0.00220* | | | *0.02990* | | | | | | | |
| Plag | = | 0.0529 | - | 0.0807 | (P) | + | 2.11 | (1-Mg#) | + | 0.343 | (NaK#) | + | 0.00140 | ($H_2O$) | - | 0.124 | ($Cr_2O_3$) | | | | -179.0 | 0.772 | 0.042 |
| | | *0.1098* | | *0.0208* | | | *0.35* | | | *0.121* | | | *0.00340* | | | *0.047* | | | | | | | |
| Qz | = | 0.474 | - | 0.0612 | (P) | - | 1.38 | (1-Mg#) | - | 0.0691 | (NaK#) | + | 0.00840 | ($H_2O$) | + | 0.0307 | ($Cr_2O_3$) | | | | -239.6 | 0.553 | 0.026 |
| | | *0.069* | | *0.0131* | | | *0.22* | | | *0.0757* | | | *0.00210* | | | *0.0291* | | | | | | | |

[a]Data in Table 4

[b]AIC = Akaike Information Criteria (Akaike, 1974); Numbers in italics are the standard errors for the coefficients presented.

[c]For each regression, the difference is calculated between the real and predicted value of each data point. The average of these differences is the mean absolute error.

Units: P (GPa), 1-Mg# (1-($X_{Mg}$/($X_{Mg}$+$X_{Fe}$)) -calculated using moles), NaK# (($Na_2O$+$K_2O$/($Na_2O$+$K_2O$+CaO)) - calculated using wt% oxides), $H_2O$ (wt%), $TiO_2$ (wt%), $Cr_2O_3$(wt%)

**Table 7** Natural HMMBAA Samples and Model $H_2O$ Contents at 1.0, 1.5 GPa

| Reference | Location | Natural Lavas | $H_2O$ at 1.0 GPa[a] | $H_2O$ at 1.5 GPa[b] |
|---|---|---|---|---|
| Bryant et al. (2010) | Kamchatka | SHISH0401 | 3.5 | 6.1 |
| | | SHISH0408 | 3.2 | 5.8 |
| | | SHISH0402 | 4.0 | 6.6 |
| | | SHISH0405 | 3.9 | 6.5 |
| | | SHISH0404 | 4.8 | 7.5 |
| | | SHISH0409 | 5.0 | 7.6 |
| Tatsumi and Ishizaka (1982) | Setouchi | TGI | 6.5 | 9.1 |
| | | TGI-6 | 6.2 | 8.9 |
| | | TGI-5 | 6.2 | 8.8 |
| | | WS 17.1 | 5.1 | 7.8 |
| | | WS-17.2 | 4.8 | 7.5 |
| | | WS-7.2 | 7.2 | 9.8 |
| | | TK-52 | 5.5 | 8.2 |
| | | SD-249 | 6.2 | 8.9 |
| | | NBY-11 | 4.0 | 6.6 |
| | | HG-130 | 2.9 | 5.6 |
| Baker et al. (1994) | Cascades | 85-1a | 3.7 | 6.4 |
| | | 85-1b | 4.0 | 6.6 |
| | | 85-41c | 5.6 | 8.3 |
| | | 82-94a | 3.6 | 6.2 |
| | | 82-94b | 3.8 | 6.4 |
| | | 82-94c | 4.0 | 6.6 |
| | | 82-81 | 4.3 | 7.0 |
| | | 85-5 | 3.9 | 6.5 |
| | | 85-44 | 4.3 | 7.0 |
| | | 85-45 | 3.6 | 6.3 |
| | | 85-46 | 4.1 | 6.7 |
| Grove et al. (2002) | Cascades | 95-15 | 3.3 | 5.9 |
| | | 97-2 | 3.8 | 6.5 |
| Barr et al. (in prep) | Cascades | 07-28 | 4.7 | 7.4 |
| Meriggi et al. (2008); Weber et al. (2011) | TMVB[c] | d-25 | 5.2 | 7.8 |
| Weaver et al. (2011) | TMVB | JR-28 | 4.8 | 7.4 |

[a] $H_2O$ contents predicted by the model when pressure is fixed at 1.0 GPa.

[b] $H_2O$ contents predicted by the model when pressure is fixed at 1.5 GPa.

[c] Trans-Mexico Volcanic Belt.